The 2019 Raikoke volcanic eruption: Part 1 Dispersion model simulations and satellite retrievals of volcanic sulfur dioxide

Johannes de Leeuw[1], Anja Schmidt[1,2], Claire S. Witham[3], Nicolas Theys[4], Isabelle A. Taylor[5], Roy G. Grainger[5], Richard J. Pope[6,7], Jim Haywood[3,8], Martin Osborne[3,8], and Nina I. Kristiansen[3]

[1]Department of Chemistry, University of Cambridge, Cambridge, UK.
[2]Department of Geography, University of Cambridge, Cambridge, UK.
[3]Met Office, Exeter, UK
[4]Royal Belgian Institute for Space Aeronomy (BIRA-IASB), Brussels, Belgium.
[5]COMET, Sub-Department of Atmospheric, Oceanic and Planetary Physics, University of Oxford, Oxford, UK
[6]School of Earth and Environment, University of Leeds, Leeds, UK.
[7]National Centre for Earth Observation, University of Leeds, Leeds, UK.
[8]College of Engineering, Mathematics, and Physical Sciences, University of Exeter, Exeter, UK.

Correspondence: Johannes de Leeuw (jd876@cam.ac.uk)

Abstract. Volcanic eruptions can cause significant disruption to society and numerical models are crucial for forecasting the dispersion of erupted material. Here we assess the skill and limitations of the Met Office's Numerical Atmospheric-dispersion Modelling Environment (NAME) in simulating the dispersion of the sulfur dioxide (SO_2) cloud from the 21-22 June 2019 eruption of the Raikoke volcano (48.3°N, 153.2°E). The eruption emitted around 1.5 ± 0.2 Tg of SO_2, which represents the

5   largest volcanic emission of SO_2 into the stratosphere since the 2011 Nabro eruption. We simulate the temporal evolution of the volcanic SO_2 cloud across the Northern Hemisphere (NH) and compare our model simulations to high-resolution SO_2 measurements from the Tropospheric Monitoring Instrument (TROPOMI) and the Infrared Atmospheric Sounding Interferometer (IASI) satellite SO_2 products.

We show that NAME accurately simulates the observed location and horizontal extent of the SO_2 cloud during the first

10 2-3 weeks after the eruption, but is unable, in its standard configuration, to capture the extent and precise location of very high-concentration regions within the volcanic cloud. Using the Fractional Skill Score as metric for model skill, NAME shows skill in simulating the horizontal extent of the cloud for 12-17 days after the eruption where vertical column densities (VCD) of SO_2 (in Dobson Units, DU) are above 1 DU. For SO_2 VCDs above 20 DU, which are predominantly observed as small-scale features within the SO_2 cloud, the model shows skill on the order of 2-4 days only. The lower skill for these high-concentration

15 regions is partly explained by the model-simulated SO_2 cloud in NAME being too diffuse compared to TROPOMI retrievals. Reducing the standard diffusion parameters used in NAME by a factor of four results in a slightly increased model skill during the first five days of the simulation, but on longer timescales the simulated SO_2 cloud remains too diffuse when compared to TROPOMI measurements.

We find that the temporal evolution of the NH-mean SO_2 mass burden simulated by NAME strongly depends on the fraction

20 of SO_2 mass emitted into the lower stratosphere, which is uncertain for the 2019 Raikoke eruption. When emitting 0.9-1.1 Tg of SO_2 into the lower stratosphere (11-18 km) and 0.4-0.7 Tg into the upper troposphere (8-11 km), both NAME and

TROPOMI show a similar peak in SO_2 mass burden (1.4-1.6 Tg of SO_2) with an average SO_2 e-folding time of 14-15 days in the NH.

Our work demonstrates the large potential of using high-resolution satellite retrievals to identify and rectify limitations in dispersion models like NAME, which will ultimately help to improve dispersion modelling efforts of volcanic SO_2 clouds.

1 Introduction

Volcanic activity can vary strongly in intensity, ranging from passive degassing volcanoes emitting sulfur into the lower troposphere to explosive eruptions that can release large amounts of ash and gases high into the stratosphere (e.g., Oppenheimer et al., 2011). It is well established that volcanic eruptions can impact Earth's climate system through changes in the energy balance (e.g., Robock, 2000; Schmidt et al., 2012; Stenchikov, 2016; Schmidt et al., 2018), which can affect the hydrological cycle (e.g., Trenberth and Dai, 2007) and atmospheric dynamics (e.g., Shindell et al., 2004). Furthermore, volcanic air pollution events can lead to a severe and spatially widespread health hazard and increase excess mortality (e.g., Schmidt et al., 2011).

For the aviation industry, ash and gas emissions from volcanic eruptions can pose a flight safety hazard. Flying through volcanic ash is a well-recognised hazard as it can reduce visibility, damage the exterior of the aircraft and compromise the functionality of aircraft engines. Ingestion of volcanic ash can cause engine failure and permanently damage jet engines (Casadevall et al., 1996; Prata and Tupper, 2009; Dunn, 2012; Prata et al., 2019). When sulfur dioxide (SO_2) oxidises to sulfuric acid and upon hydration forms sulfuric acid aerosol particles (see e.g., Hamill et al., 1977; Hofmann and Rosen, 1983), damage to the exterior of aircrafts can occur (e.g. window crazing) (Bernard and Rose, 1990). Through sulfidation, SO_2 can also cause serious damage to the interior of the engines. Sulfuric acid aerosol particles have been recorded to corrode nickel alloys in engine components (e.g. compressor blades) when alkali metal salts, like mineral dust or sea salt, are co-present (Eliaz et al., 2002; Grégoire et al., 2018). While this effect has not been linked to immediate engine failures, it is a concern for the aviation industry as it increases maintenance costs. Apart from material damage, sulfurous odours can also cause distress of cabin passengers and aircrew.

The Raikoke volcano is located in the Kuril Island chain, near the Kamchatka Peninsula in Russia (48.3°N, 153.2°E, see fig. 1) and had been dormant since 1924. On June 21, 2019 at 1800 UTC Raikoke started erupting and continued erupting until about 0300 UTC on 22 June, 2019). During this period, Raikoke released the largest amount of SO_2 into the stratosphere since the Nabro eruption in 2011 (Goitom et al., 2015). The volcanic cloud (while a geographic distribution of SO_2 and/or sulfate aerosol is not technically a cloud in the meteorological sense, we use this term through our paper as it is common practice in the atmospheric dispersion community.) dispersed across the Northern Hemisphere (NH) within the first few weeks after the eruption and was observed by various ground-based observational networks (e.g., Vaughan et al., 2020; Mateshvili et al., 2020), aircraft-based instruments (e.g., Bundke et al., 2020) and satellites (e.g., Muser et al., 2020) in the following months.

The International Airways Volcanic Watch (IAVW) is responsible for the dissemination of information on the occurrence of volcanic eruptions and associated volcanic ash clouds (ICAO, 2019a) through nine Volcanic Ash Advisory Centres (VAACs). During a volcanic eruption the responsible VAAC disseminates relevant information to the aviation sector regarding the ge-
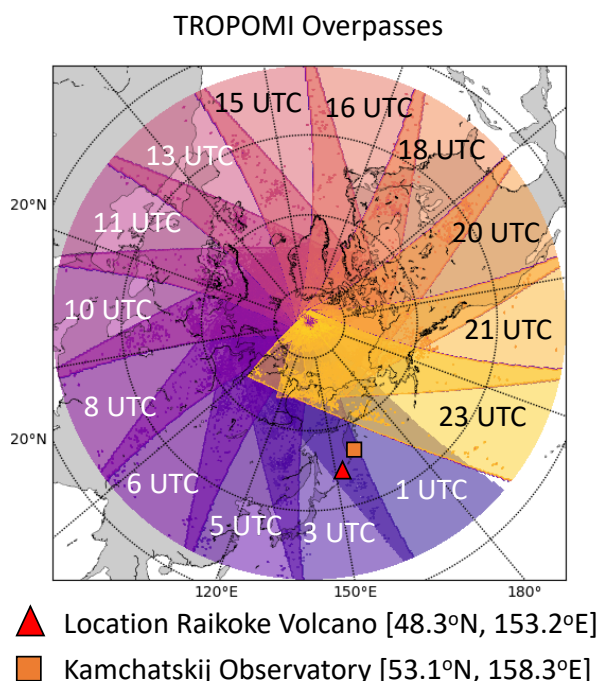
Figure 1. Example of daily TROPOMI overpasses (north of $25°$N, with a swath width of 2600 km). Time indicates the approximate central time for each overpass (each track takes approximately 1.5-2 hours). Note the overlap of the swaths, resulting in a higher temporal resolution near the pole. Also shown are the location of the Raikoke volcano (triangle) and the radiosonde location at the Kamchatskij Airport (square).

55 ographic location of volcanic ash present in the atmosphere. Currently, the VAACs are only required to provide forecasts of volcanic ash dispersion and therefore less development has been made on the forecasting of volcanic gas clouds. There is, however, increasing consensus among the scientific community that monitoring and simulating SO_2 clouds could be of interest to stakeholders, as volcanic SO_2 can pose a public health hazard and potentially affect the aviation industry (e.g. increase of aircraft maintenance costs) (Witham et al., 2012; Schmidt et al., 2014; Carboni et al., 2016; Granieri et al., 2017; Grégoire

60 et al., 2018). Volcanic SO_2 clouds are also frequently (but not always) co-located with ash clouds. Detecting ash clouds from satellites retrievals remains a challenging task and therefore SO_2 clouds are potential tracers for the more difficult observable ash clouds (e.g., Sears et al., 2013; Kristiansen et al., 2015). As a result, the latest roadmap published by the IAVW (ICAO, 2019b) includes SO_2 forecasts as a core item to be implemented in the future.

The main tool used by VAACs to provide accurate forecasts of volcanic cloud characteristics is atmospheric dispersion

65 models (ADMs), which are numerical models that simulate how air parcels disperse within the atmosphere. ADMs are used for a large variety of advection-related research, including dust transport, nuclear accidents, forest fires, air pollution, plant diseases and volcanic clouds (Carpenter et al., 2010; Webster et al., 2011; Katata et al., 2014; Schmidt et al., 2014, 2015; Ashfold et al., 2017; Meyer et al., 2017; Osborne et al., 2019). Because of the ash-focused task of VAACS, there has been

a strong research focus on improving the simulation of volcanic ash in ADMs and measuring volcanic ash using in-situ and satellite measurement techniques (e.g., Witham et al., 2007; Corradini et al., 2011; Prata and Prata, 2012; Mulena et al., 2016; Harvey et al., 2018; Webster et al., 2020). The skill of ADMs in simulating the evolution of SO_2 clouds has also been investigated (e.g., Eckhardt et al., 2008; Heard et al., 2012; Boichu et al., 2013; Schmidt et al., 2015), but to a much lesser extent as this has generally been the realm of global climate models interested in the climatic impacts of the periodic stratospheric injections from volcanoes (e.g., Haywood et al., 2010; Solomon et al., 2011; Schmidt et al., 2018).

Observations are vital in determining the skill of the dispersion models. While in situ observations are available for several well-studied volcanoes (e.g., Pfeffer et al., 2018; Sahyoun et al., 2019; Whitty et al., 2020), they are only available for a limited number of locations. In recent decades, many high-resolution remote-sensing measurements have become available, providing a great data source on activity at even the most remote volcanoes across the globe. A large number of satellites now measure atmospheric SO_2, with each newly launched instrument having an increased accuracy (see for example fig. 2 in Theys et al. (2019)). The TROPOspheric Monitoring Instrument (TROPOMI), which is part of the ESA's S5P satellite, has been operational since the end of 2017 and measures atmospheric SO_2 concentration at an unprecedented resolution (Theys et al., 2017, 2019). TROPOMI therefore provides a useful new source of information to evaluate model simulations of SO_2 clouds using ADMs (and climate models).

One major issue for the development of ADMs for volcanic clouds is the relatively small number of large-magnitude eruptions available since the start of the satellite era in 1979 in order to validate model output. While smaller-magnitude eruptions take place more frequently, large-magnitude eruptions that can emit large amounts of SO_2 into the stratosphere are much more sporadic (e.g., Pyle, 1995; Carn et al., 2016; Schmidt et al., 2018). The 2019 Raikoke eruption is the first eruption with SO_2 emissions in excess of 1 Tg of SO_2 that has been observed by the TROPOMI instrument. Because of the amount of SO_2 emitted into the stratosphere, it provides an ideal test case to validate the skill of the Numerical Atmosphere-dispersion Modelling Environment (NAME) (Jones et al., 2007), which is the dispersion model used by the London VAAC (Witham et al., 2020). In this paper we will focus on the evolution of the volcanic SO_2 cloud during the first 3 weeks after the 2019 Raikoke eruption and compare the output from NAME with the TROPOMI and the Infrared Atmospheric Sounding Interferometer (IASI) satellite SO_2 products. In the accompanying Part 2 paper (Osborne et al., 2020), a detailed assessment of the sulfate aerosol together with volcanic ash from this eruption are discussed as well as the effects from biomass burning aerosols that were emitted into the stratosphere from an unusually strong pyrocumulus event in continental north America.

The manuscript is structured as follows: after discussing the TROPOMI and the IASI satellite SO_2 products in sections 2.1 and 2.2, we briefly introduce all the relevant aspects of the NAME dispersion model in section 2.3. As part of this discussion, we present three vertical SO_2 emission profiles in sections 2.3.5 that we used for our NAME simulations, one of which is derived from combining the TROPOMI satellite SO_2 products and an initial 36 hour NAME simulation. Using the introduced input parameters for our 25-day long NAME simulations, we obtain a good qualitative comparison of the simulated SO_2 cloud with the TROPOMI satellite SO_2 products during the first 3 weeks after the eruption, which we present in section 3.1. A more detailed analysis of the model skill is presented in sections 3.2 and 3.3, where we show that the Fractional Skill Score (FSS) and the SAL-score (both metrics are introduced in section 2.4) are powerful tools for assessing the skill of the model simulations in

comparison to satellite measurements. The NAME simulation skill in terms of the NH-mean SO_2 mass burden throughout the

105   first 25 days after the Raikoke eruption are presented in section 3.4, showing a large dependence of the mass burden evolution on the vertical emission profile. We will finish with a discussion of our work (section 4) and present the main conclusions in section 5.

2   Data and Methods

2.1   TROPOspheric Monitoring Instrument

110   TROPOMI is part of the ESA's S5P satellite launched on 13 October 2017 (Veefkind et al., 2012) and is a polar-orbiting, sun-synchronous, hyperspectral spectrometer that measures Earth reflected radiances in the ultraviolet (UV), visible, near-infrared and shortwave infrared parts of the spectrum. Atmospheric SO_2 vertical column density (VCD, expressed in Dobson units with $1\,DU = 2.69 \times 10^{16}\,\mathrm{molecules\,cm^{-2}}$) is retrieved by applying Differential Optical Absorption Spectroscopy (DOAS) (Platt and Stutz, 2008) to the measured ultraviolet spectra in three wavelength ranges ($312\,nm$ - 326 nm, $325\,nm$ - $335\,nm$,

115   and $360\,nm$ - $390\,nm$). For a more detailed description of the SO_2 retrieval, we refer the reader to Theys et al. (2017) and Theys (2018).

    In our study we use the TROPOMI satellite retrievals across the northern hemisphere (north of 25° N) that cover the Raikoke SO_2 cloud between 22 June and 15 July 2019. Figure 1 shows an example of the TROPOMI daily overpasses over the northern hemisphere. Compared to its predecessors OMI and SCIAMACHY, TROPOMI has a higher horizontal pixel resolution (up to

120   3.5 km $\times$ 5.5 km), allowing for a more detailed characterisation of the small-scale features in volcanic SO_2 clouds (Theys et al., 2019). The retrieved TROPOMI SO_2 VCD product is calculated by accounting for a large number of parameters, such as meteorological cloud fraction, surface albedo and the vertical distribution of absorbing trace gases (e.g. ozone) (Theys et al., 2017; Theys, 2018). As a result, the SO_2 retrievals from TROPOMI are sensitive to many assumptions which can lead to uncertainties of up to $\pm 50\%$. For SO_2 in the stratosphere, the sum of the various uncertainties can be approximated to be

125   around of ± 30 % of the retrieved SO_2 VCDs. For a detailed discussion of the retrieval uncertainties see Theys et al. (2017).

    One of the largest uncertainties of the TROPOMI SO_2 VCD product is the height of the SO_2 cloud. However, the sensitivity of the measurement with height is well characterised. The most reliable method to compare satellite retrievals with any atmospheric dispersion model output is by applying the column Averaging Kernel (AK) operator to the model data, thereby matching the model SO_2 VCDs to the TROPOMI product. The AKs are obtained alongside the TROPOMI SO_2 VCD product

130   (Theys, 2018). The TROPOMI VCD data presented in this study is calculated assuming that the SO_2 layer is at 15 km above ground level (agl). We have applied the corresponding column AK operator to the NAME simulation output, thereby enabling a one-to-one comparison. We have repeated the analysis using the AKs for an SO_2 layer at 7 km agl in TROPOMI, which affects the absolute SO_2 VCDs (not shown), but not our interpretation of the results or our overall conclusions.

    To obtain a daily SO_2 mass estimate from the TROPOMI measurements, we grid the satellite data and combine all the

135   overpasses during a 24-hour period starting at 12 UTC of any given day. In the case of multiple overpasses over a single location, we average the SO_2 cloud at these grid locations to avoid double counting. For the mass estimate from TROPOMI

we have used a detection threshold of 0.3 DU. The resulting VCD (in DU) is then converted into a mass (Tg) by using the area of each individual grid point and the molar mass of SO_2. Due to the high spatial resolution of the TROPOMI retrieval (on average nine TROPOMI pixels per output grid cell for the resolution used in the dispersion model), we have down-scaled the

140 final TROPOMI retrievals to the resolution of the NAME dispersion model by averaging the VCDs of all pixels within each NAME grid cell ($0.2°$latitude $\times$ $0.4°$longitude). Unless otherwise specified, we refer to the sulfur dioxide mass burden as the total SO_2 mass within the northern hemisphere, north of $25°$ N.

During the initial stage of the eruption, it is likely that TROPOMI underestimates the SO_2 VCDs due to the presence of volcanic ash (e.g., Yang et al., 2010). To understand if ash-inference is likely to have affected our SO_2 estimates, we also

145 retrieve the absorbing aerosol index (AAI) from the TROPOMI instrument (Zweers, 2016). Although the TROPOMI AAI product should be used with care (see e.g., de Graaf et al., 2016; Kooreman et al., 2020), high index values (> 1) can indicate the presence of aerosol plumes from dust outbreaks, volcanic ash, and biomass burning. During the first 48 hours after the eruptions we found high peak AAI values within the volcanic cloud (> 18.9 on the 22 June and > 3.5 on the 23 June), indicating that volcanic ash had an impact on the SO_2 retrieval during this period.

150 ## 2.2 The Infrared Atmospheric Sounding Interferometer

The second satellite SO_2 dataset used in our analysis is acquired using IASI onboard of the Metop-A and Metop-B satellites. These satellites operate in tandem on a polar orbit with a field-of-view (FOV) consisting of four circular footprints of 12 km diameter (at nadir) inside a square of 50 km $\times$ 50 km and provide a global coverage twice a day. For our analysis we use the SO_2 plume height estimates based on the IASI data, which is produced by applying the retrieval algorithm presented in

155 Carboni et al. (2012) and Carboni et al. (2016). The IASI instrument also retrieves the SO_2 VCDs within the volcanic plume, but uses a different set of assumptions in the retrieval algorithm (e.g. plume height) compared to TROPOMI. To compare SO_2 VCDs from NAME to the IASI data, one would therefore also need to apply a different scaling (i.e. AK). As the TROPOMI and IASI retrieval assumptions are satellite-specific, a comparison between the two VCD products is not straightforward and is not attempted here. While it would be an interesting exercise to apply our analysis also to the IASI data, we focus on the

160 comparison of NAME with the TROPOMI SO_2 estimates and therefore no further analysis is done for the IASI VCD retrievals.

2.3 Numerical Atmosphere-dispersion Modelling Environment (NAME)

The Numerical Atmospheric-dispersion Modelling Environment (NAME) is developed by the Met Office (Jones et al., 2007) and is the operational dispersion model used by the London VAAC to forecast the dispersion of volcanic clouds within European Airspace (e.g. the Icelandic eruptions of Eyjafjallajökull in 2010 and Holuhraun in 2014-2015). For our work we use NAME

165 version 8.0. The model can trace both ash particles and gases through the atmosphere and includes chemistry parameterisations that allow the conversion of SO_2 into sulfate aerosols (SO_4) within the volcanic cloud. (see section 2.3.3). There is no radiative nor chemical interaction between the ash particles and the sulfur species in NAME; the ash particles and sulfate aerosols are thus considered to be externally mixed. In this section we focus on the dispersion of SO_2 and highlight the important aspects

of NAME for this part of the research. More details on the modelling of ash particles within the model are discussed in the
170   accompanying Part 2 paper (Osborne et al., 2020).

2.3.1   Simulating volcanic cloud dispersion using NAME

Simulating the dispersion of a volcanic cloud with NAME relies on the tracing of air parcels through the atmosphere, each
containing an ash, SO_2 and/or SO_4 mass. These air parcels are released from the 'source' location (volcano), where the user
has to define the eruption source parameters (see section 2.3.4). NAME is an offline model, therefore each parcel is advected
175   by an externally obtained wind field (e.g. a high resolution Numerical Weather Prediction (NWP) model). In our simulations,
we use the wind fields from the latest Global analysis of the Met Office Unified Model (MetUM), which have a horizontal
resolution of around $10 \, \mathrm{km}$ at mid-latitudes, 59 levels between the surface and 30 km asl and a 3 hourly temporal resolution.

The path of each trajectory is calculated using the following equation:

$$\boldsymbol{x}(t + \Delta t) = \boldsymbol{x}(t) + [\boldsymbol{u}(\boldsymbol{x}(t)) + \boldsymbol{u}'(\boldsymbol{x}(t))]\Delta t, \tag{1}$$

180   where $\boldsymbol{x}(t)$ is the location of the parcel at time t, $\boldsymbol{x}(t + \Delta t)$ the new location of the parcel at time $t + \Delta t$, $\boldsymbol{u}(\boldsymbol{x}(t))$ the 3D-
wind vector at location $\boldsymbol{x}(t)$ and $\boldsymbol{u}'(\boldsymbol{x}(t))$ represents a stochastic perturbation to the parcels trajectory representing turbulence
and unresolved sub-grid mesoscale wind variations in the dispersion model. In NAME, $\boldsymbol{u}'$ consists of two parts representing
atmospheric turbulence ($\boldsymbol{u}'_{turb}$) and sub-grid mesoscale diffusion ($\boldsymbol{u}'_{meso}$). The turbulence part represents the stochastic mo-
tions from the air parcels due to small-scale perturbations. The mesoscale diffusion represents the mesoscale motions in the
185   atmosphere that are not captured by the resolution of the used NWP model. Each NWP has a limited spatial and temporal
resolution and as a result, part of the mesoscale features (e.g. eddies) are not captured by the NWP wind field provided. Both
the turbulence and mesoscale diffusion within the free atmosphere (excluding the Planetary Boundary Layer, which has a more
detailed scheme (Webster et al., 2018)) are calculated using:

$$\boldsymbol{u}'_{turb}\Delta t = r\sqrt{2\boldsymbol{K_{turb}}\Delta t}, \tag{2}$$

190    $$\boldsymbol{u}'_{meso}\Delta t = r\sqrt{2\boldsymbol{K_{meso}}\Delta t}, \tag{3}$$

$$\boldsymbol{K_x} = (\sigma_u^2 \tau_u, \sigma_v^2 \tau_v, \sigma_w^2 \tau_w), \tag{4}$$

where $\boldsymbol{K_x}$ is a 3D-diffusion vector defined separately for both components, using typical velocity and time length-scales σ
and τ for the described perturbations. r represents a random number from a top-hat distribution within the range [-1,1]. The
values for σ and τ are dependent on the NWP model used, as it is impacted by the resolution of the model (Harvey et al., 2018;
195   Webster et al., 2018). The values for σ and τ used in this study are obtained from the analysis done by Webster et al. (2018)
and are shown in table 1. Note that for. $\boldsymbol{K_{meso}}$ the vertical component ($\sigma_w^2 \tau_w$) is zero.

To investigate the importance of the mesoscale diffusion parameter, we conduct two sensitivity simulations with two different
SO_2 emissions profiles (see section 2.3.4 for discussion of these profiles) and a reduced value for $\boldsymbol{K_{meso}}$ (see table 2). These
simulations are indicated by the subscript $_{rd}$ throughout this study.

Table 1. The values for the diffusion parameter K used in NAME. Values are NWP dependent and are given here for the Met Office Unified Model Global analysis (10 km horizontal resolution, 59 levels) with a 3 hourly temporal resolution. Values for σ^2 are given instead of σ to be consistent with the values presented by Webster et al. (2018). Values are given for both the turbulence K_{turb} and the mesoscale diffusion K_{meso} that are used in NAME for the free atmosphere (i.e. excluding the boundary layer).

Global MetUM analysis ($0.140625° \times 0.09375°$, 59 levels, 3 hourly resolution)

	K (m^{2}s^{-1})	$\sigma_{u,v}^2$ (m^{2}s^{-2})	$\tau_{u,v}$ (s)	σ_w^2 (m^{2}s^{-2})	τ_w (s)
K_{turb}	(18.75,18.75,1)	0.0625	300	0.01	100
K_{meso}	(6400,6400,0)	0.64	10000	0	0

2.3.2 Calculating SO$_2$ mass estimates from NAME

In our simulations, the SO$_2$ concentrations from all the individual air parcels in NAME are presented as hourly-means on a regular latitude-longitude grid by calculating the total mass of the SO$_2$ of all parcels in each grid box every hour. The NAME output is calculated using a grid size of $0.2°$ latitude and $0.4°$ longitude (approximately 20 km $\times$ 20 km at the latitude of the Raikoke volcano). The vertical resolution of the output is 500 m up to 15 km agl and 1 km resolution up to 20 km agl, giving a total of 35 levels.

To compare the daily SO$_2$ mass estimates from NAME and TROPOMI, we select the hourly NAME output corresponding to each individual TROPOMI overpass time and select only the grid boxes in NAME that are in the domain scanned by TROPOMI during that overpass. To calculate the SO$_2$ VCD, we apply the corresponding column AK operator obtained from TROPOMI (see section 2.1) to each grid cell of the NAME output. After multiplying each grid cell value by the area of the grid cell and summing the resulting mass in each column we obtain the VCDs estimate from NAME.

In all our NAME simulations we found that the SO$_2$ cloud is more diffuse than observed by TROPOMI. Therefore, removing all VCDs <0.3 DU in NAME (which is the detection threshold used for TROPOMI, see section 2.1) from the simulations would result in a negative bias within the NAME simulation mass estimates that are not related to the evolution of the cloud, but due to the stronger diffusion within the model. Therefore we have not included a detection threshold when determining the SO$_2$ mass estimates for the NAME simulations. Similarly to the TROPOMI estimate, the daily mass estimates from NAME are calculated during a 24-hour period starting at 12 UTC of any given day. The SO$_2$ mass burden is defined as the total SO$_2$ mass (Tg) within the NH, north of $25°$ N.

2.3.3 Chemistry within NAME

NAME contains an atmospheric chemistry scheme (Redington et al., 2009). The relevant chemistry for volcanic clouds is related to the conversion of SO$_2$ into sulfate (SO$_4^{2-}$). NAME accounts for the oxidation of SO$_2$ in the gas phase using the following reaction

$$OH + SO_2 + M \rightarrow HSO_3 + M \tag{R1}$$

where HSO_3 is then rapidly oxidised to H_2SO_4 on formation. When water is present in the atmosphere, the oxidation can happen in the aqueous phase by both H_2O_2 and O_3 through the following reaction:

$$SO_2 + H_2O \quad \rightleftharpoons \quad H^+ + HSO_3^- \tag{R2}$$

$$HSO_3^- \quad \rightleftharpoons \quad H^+ + SO3^{2-} \tag{R3}$$

which is followed by

$$HSO_3^- + H_2O_2 \quad \rightarrow \quad SO_4^{2-} + H^+ + H_2O \tag{R4}$$

$$HSO_3^- + O_3 \quad \rightarrow \quad SO_4^{2-} + H^+ + O_2 \tag{R5}$$

$$SO3^{2-} + O_3 \quad \rightarrow \quad SO_4^{2-} + O_2 \tag{R6}$$

Reactions R2-R6 dominate in cloudy conditions and only occur in model grid boxes when both the cloud fraction and liquid water content are non-zero. The concentrations of H_2O_2 and O_3 in the atmosphere are pre-defined in the NAME model by using monthly-mean background fields obtained from a historical UM-UKCA model (Unified Model coupled to the United Kingdom Chemistry and Aerosol model) simulation that have been smoothed between months using interpolation.

In NAME the SO_2 and sulfate aerosol particles can be removed through dry and wet deposition. For our simulations we found that the dry deposition had limited importance for the 2019 Raikoke eruption as most of the volcanic clouds are at high altitudes. Wet deposition in NAME is calculated using a standard depletion equation:

$$\frac{dC}{dt} = \Lambda C \tag{5}$$

$$\Lambda = Ar^B \tag{6}$$

with C representing the SO_2 air concentration and Λ the scavenging coefficient, which is calculated based on the rainfall rate r (in mm/hr) and two scavenging parameters A and B. The parameters A and B vary for different types of precipitation (i.e., large-scale/convective and rain/snow) and for different wet deposition processes (i.e., rainout, washout and the seeder-feeder process). For more detailed information, including the values for A and B, we refer to Leadbetter et al. (2015) and references therein.

2.3.4 Eruption Source Parameters

When simulating a volcanic eruption, the NAME dispersion model needs eruption source parameters (ESP) consisting of 1) location, 2) timing, 3) mass flux and 4) vertical emission profile, and for simulating volcanic ash also 5) particle density, shape and particle size distribution. Here we will discuss ESP 1-4. For information about the setup of the simulations including ash, we refer to the Part 2 paper (Osborne et al., 2020). For all simulations described in this manuscript, we released a total of 10 million air parcels in NAME within a column above the volcano, each parcel representing an equal amount of SO_2 mass. All simulations are run for 25 days until 15 July 2019.

In all our simulations (see table 2 for overview), we release the SO_2 from the location of the volcano (48.3° N, 153.2° E) between 21 June 18 UTC and 22 June 03 UTC. As there is very limited information available about the temporal variation in

Table 2. Overview of the NAME simulations performed using different emission profiles and a reduced mesoscale diffusion. Also shown is the estimated mass emitted into the stratosphere. For the actual vertical emission profiles, please see fig. 2. All the simulations use the same NWP data input (Global MetUM), the same emission location ($48.3°$ N, $153.2°$ E), emission duration (21 June 1800 UTC - 22 June 0300 UTC 2019) and simulation length (25 days).

Simulation name	Mass emitted	Profile used	Mass Stratosphere	Mesoscale diffusion
VolRes1.5	1.5 Tg	VolRes1.5	0.64 Tg	full
VolRes2.0	2.0 Tg	VolRes2.0	0.85 Tg	full
StratProfile	1.57 Tg	StratProfile	1.09 Tg	full
VolRes1.5$_{rd}$	1.5 Tg	VolRes1.5	0.64 Tg	0.25 $\boldsymbol{K_{meso}}$
StratProfile$_{rd}$	1.57 Tg	StratProfile	1.09 Tg	0.25 $\boldsymbol{K_{meso}}$
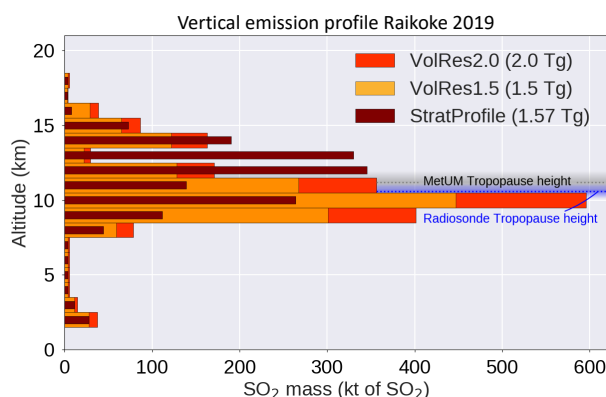
Figure 2. Estimated total emitted SO_2 mass for the Raikoke eruption between 21 June 1800 UTC and 22 June 0300 UTC 2019. The initial emission profile was provided by the VolRes (Volcano Response) team, which is implemented in NAME for the 1.5 Tg SO_2 simulation (VolRes1.5, orange). We also simulated the same profile for a 2.0 Tg SO_2 emission (VolRes2.0, red). Also included is a new emission profile estimate (StratProfile, brown) based on the TROPOMI VCD cloud on 23 June (see section 2.3.5). This profile has a similar total mass emitted to VolRes1.5, but a larger fraction (69% instead of 43%) of its mass is emitted in the stratosphere (see table 2). The grey line represents the average tropopause height in the MetUM during the first 36 hours after the eruption at the location of Raikoke volcano. The blue line and shading represents the average and the range of measured tropopause heights by the radiosondes released from the Kamchatskij Observatory (square in fig. 1) during the first 36 hours after the eruption.

the mass eruption rate, we assume a constant mass flux throughout the entire eruption period. For the vertical profile we use

255 three different estimates as shown in fig. 2. The first SO_2 emission profile is based on the distribution obtained from the Volcano Response (VolRes) team (https://wiki.earthdata.nasa.gov/display/volres). The VolRes team is an international research collaboration to coordinate a response plan after large volcanic eruptions using observational and modelling tools. For the Raikoke eruption the VolRes team documented a best estimate of the mass-altitude distribution derived from the IASI measurements on 22 June, as shown by the orange bars in fig. 2. The emission profile peaks at 10 km altitude, with a secondary peak at 14

260 km agl. The total SO_2 mass emitted based on the VolRes estimate was approximately 1.5 ± 0.2 Tg of SO_2, of which 43% was released into the lower stratosphere.

To investigate the impact of the emission profile on the results, apart from the initial run (VolRes1.5), we also conduct a sensitivity simulation in which we released a total of 2 Tg of SO_2, using the same profile shape (VolRes2.0). In addition, we derive a different vertical profile based on the TROPOMI SO_2 VCD cloud (StratProfile, see section 2.3.5). Different from the

265 VolRes profiles (which are based on the IASI satellite overpasses on 22 June), our TROPOMI estimated profile is based on the 23 June overpasses, as this reduced the interference of ash during the initial stages of the eruption (see section 2.1) and also showed relatively modest VCDs compared to previous overpasses of TROPOMI. The derived StratProfile profile releases similar amounts of SO_2 into the atmosphere as the VolRes1.5 run (1.57 Tg), but a much higher fraction (69%) of the mass is released into the lower stratosphere with the main peak in SO_2 mass at 12-13 km altitude.

270 To understand what fraction of the total mass was emitted into the stratosphere, we calculated the tropopause height in the MetUM global analysis using the World Meteorological Organization (WMO) temperature lapse rate definition. Using the spread in the 150 nearest grid points to the volcano location in the model, we get an average tropopause height of 11.2 ± 0.7 km during the first 36 hours after the eruption. To verify this tropopause height, we used radiosonde data from the Kamchatskij Observatory (see fig. 1), which is the nearest radiosonde location to the Raikoke volcano (data can be retrieved from

275 http://weather.uwyo.edu/upperair/sounding.html). Using the same tropopause criteria for the radiosondes released from this location, we estimate an average tropopause altitude of 10.5 ± 0.7 km during the first 36 hours, showing that the MetUM simulated the tropopause height within the expected range.

2.3.5   Stratospheric vertical emission profile

The VolRes vertical emission profile introduced in the previous section is mainly derived from the IASI satellite overpasses

280 on 22 June 2019. During this period, there was a large amount of ash within the volcanic plume that could have influenced the accuracy of the retrievals and as a result the vertical emission profile. To understand if the VolRes emission profile is appropriate, we have run an initial 36-hour NAME simulation with the VolRes1.5 vertical emission profile input and compared the SO_2 VCD estimates (fig. 3a) with the TROPOMI retrieval on 23 June (fig. 3b). We have chosen 23 June, as these are the first TROPOMI overpasses where the interference of ash on the retrieval is significantly reduced (see section 2.1). The comparison

285 reveals that the VolRes1.5 simulation has a different longitudinal distribution compared to the TROPOMI satellite retrievals. Figure 3d shows the averaged SO_2 VCDs between 48-52°N along section I-II in fig. 3a for the clouds shown in panels a-c. Especially along the northern part of the cloud as seen in fig. 3d, we see between 170-175°E that the VolRes1.5 simulation is underestimating the VCDs from TROPOMI by up to a factor of 8.

Figure 4 shows the vertical cross section from the VolRes1.5 simulation through the SO_2 cloud along section I-II in fig. 3a,

290 together with the available estimated cloud heights from IASI for all pixels between 49-50°N. The cloud height from the IASI retrieval is estimated using the method described in Carboni et al. (2016). Figure 4 shows that the SO_2 cloud between 170-175°E is simulated in NAME between 11-14 km, which coincides with the lower stratosphere in the MetUM Global model (see fig. 2). The altitude of the SO_2 cloud for the NAME VolRes1.5 simulation along the cross section shown in fig. 4 is within
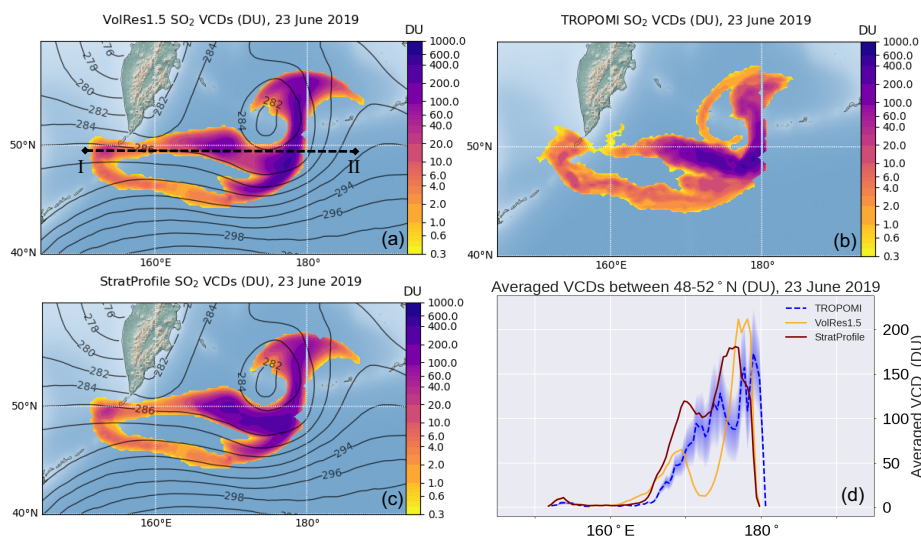
Figure 3. The SO_2 VCD estimates for 23 June 2019 for a) the VolRes1.5 simulation, b) the TROPOMI retrievals and c) the StratProfile simulation. The TROPOMI retrievals are downscaled to the NAME simulation resolution, (i.e. averaged per grid box, see sections 2.1). The black contours show the pressure at the 10 km above sea level in the MetUM analysis used for both NAME simulations. Panel d shows the latitudinal SO_2 VCDs along section I-II in fig. 3a, averaged between 48°N and 52°N for the three SO_2 clouds shown in panels a-c. Shading represent the standard error estimate for the TROPOMI estimate.
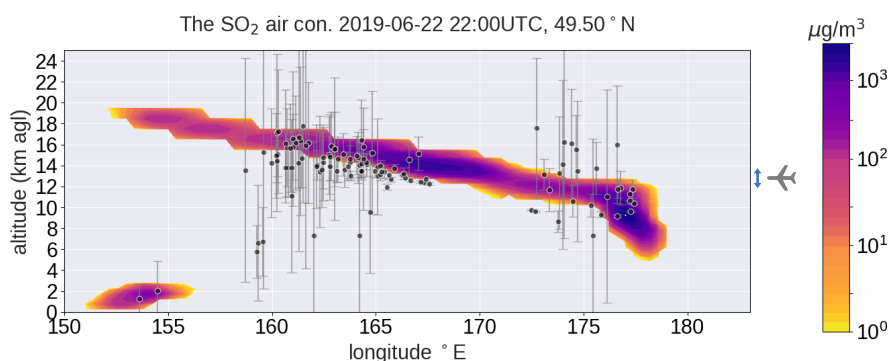
Figure 4. Vertical cross section of SO_2 mass concentrations ($\mu g/m^3$) in the VolRes1.5 simulation and the IASI height estimate along the line I-II in fig. 3a on 22 June 2019 at 22 UTC. This time corresponds with the IASI overpass over the volcanic cloud, thereby minimising displacing errors due to timing. The black dots represent the available height estimates including error bars from the IASI retrieval of the SO_2 cloud for all pixels between 49-50°N and is estimated following the method described in Carboni et al. (2016). The blue up-down arrow on the right of the figure indicates the range of cruise altitudes for heavy long-haul aircraft (11.9-13.7 km).

the uncertainty range of the IASI height estimates and gives us confidence that NAME simulated cloud heights are realistic.

295   The underestimated VCDs in the latitude range 170-175°E for the VolRes1.5 simulation (fig. 3) is therefore not due to errors in the simulated heights, but rather due to an underestimation of the fraction of SO_2 released into the stratosphere.

To investigate the sensitivity of the results to the SO_2 mass fraction that is emitted into the stratosphere, we derive a new emission profile based on the TROPOMI vertical column density on 23 June in combination with the 36-hour NAME VolRes1.5 simulation. Using fig. 3d, we scale the VolRes1.5 VCD estimates at each longitude to represent the TROPOMI VCD values

300   along cross section I-II and using fig. 4 we simultaneously derive the corresponding mass averaged cloud height for the VolRes1.5 vertical profile. The obtained scaling and altitude of the cloud at each longitude are then combined to apply a scaling to the VolRes1.5 emission profile (fig. 2). We only determine the scaling where the cloud is less than 4 km thick (between 157°E and 176°E), resulting in a scaling factor for the emission profile levels between 9 and 18 km. The resulting StratProfile shown in fig. 2 emits 1.57 Tg of SO_2 mass, which is very similar to the mass emitted by VolRes1.5. However, this

305   new profile emits a much higher fraction of the mass into the stratosphere (1.09 Tg versus 0.64 Tg, see table 2). The results for the StratProfile simulations on 23 June are presented in fig. 3c and fig. 3d and, as expected, show a better comparison with the TROPOMI satellite SO_2 VCD retrievals at this particular time. A more detailed vertical emission profile could be constructed using sophisticated inverse modelling techniques (e.g., Eckhardt et al., 2008; Kristiansen et al., 2010; Moxnes et al., 2014), but this is beyond the scope of this paper and is not attempted here.

310   ## 2.4   Metrics to determine the skill of the NAME simulations

Assessing the model's skill in representing satellite measurements of SO_2 requires appropriate metrics. Similar comparisons should be possible in almost near-real time for VAACs when investigating future eruptions. Therefore, apart from being able to show the details of the model-satellite comparison, it is also important that the metric is easily interpretable by end-users. In the following sub-sections we introduce two metrics for identifying the skill of the simulations: (1) the Fractional Skill Score

315   (FFS), and (2) the SAL-score.

2.4.1   Fractional Skill Score (FSS)

The Fractional Skill Score was originally developed to determine the skill of weather forecast models to represent radar rainfall observations (Roberts, 2008; Roberts and Lean, 2008; Mittermaier et al., 2013), but has been since used to also describe the skill of dispersion models in representing volcanic clouds (Dacre et al., 2016; Harvey and Dacre, 2016). For volcanic SO_2

320   clouds, the Fractional Skill Score is calculated using the ratio between the model-simulated (M_k) and observed (O_k) fractional coverage of the SO_2 cloud at each location (neighbourhood) in the domain investigated. When considering a neighbourhood of N grid points (or pixels), the Fractional Skill Score is calculated using:

$$FSS = 1 - \frac{FBS}{FBS_{ref}} \tag{7}$$

$$FBS = \frac{1}{N} \sum_{k=1}^{N} (O_k - M_k)^2 \tag{8}$$

325 $$FBS_{ref} = \frac{1}{N} \left[\sum_{k=1}^{N} O_k^2 - \sum_{k=1}^{N} M_k^2 \right] \tag{9}$$

The FSS is calculated from the Fractions Brier Score (FBS), which is a variation on the Brier Score (Brier, 1950), and FBS_{ref} is the largest FBS score one can obtain from multiple non-zero fractions within the domain when there is no overlap between the two fields. In the case that observations and simulation are perfectly aligned, FSS is equal to one. In the case of a total mismatch FSS equals to zero. In general for the FSS, a model-simulation is considered to have skill when FSS > 0.5 (see

330 e.g., Harvey and Dacre, 2016).

The FSS metric is very suitable for studying the skill of a model in capturing the volcanic cloud's spatial extent. One advantage of using the FSS metric is that it relaxes the requirement for exact matching of the spatial features in the simulations with the observations. Instead when the fractional coverage of the SO_2 cloud within a studied region (i.e. a neighbourhood of size N) is the same for the observations and the simulation, this metric counts it as a correct forecast. By using different

335 sizes of neighbourhoods, one can also determine at which spatial resolution the simulation is skilful (i.e. for which N is FSS > 0.5) at any given time, which helps to determine at which spatial scale features of the SO_2 cloud can be considered realistic. Note however that the method does not consider mass concentrations – it only considers a 'hit' or 'miss' for each location. By applying the same FSS metric to increasing mass concentration thresholds (i.e. sub-regions of the cloud), one can obtain information about model skill at simulating volcanic SO_2 cloud structures with varying mass densities.

340 **2.4.2 Structure, Amplitude and Location Score (SAL-score)**

The SAL-score is a metric that is composed of three components, which describe the Structure (S), Amplitude (A) and Location (L) of an investigated feature within a specified domain. The metric was originally developed to compare the structure of model-simulated precipitation fields with observations (Wernli et al., 2008), but has since been adapted to also describe other fields, including volcanic clouds (e.g., Dacre, 2011; Wilkins et al., 2016; Radanovics et al., 2018). Here we will adopt this metric to

345 describe the evolution of the SO_2 cloud. For a detailed description of the equations used to calculate each individual component we refer the reader to Wilkins et al. (2016).

Briefly, to calculate the S and L scores (not needed for the A score), we have to identify all the individual simulated and observed SO_2 clouds. In our analysis each cloud is identified as a group of adjacent grid cells which have a VCD value above a certain threshold. From Theys et al. (2019) we deduce that the detection limit of the satellite measurements for individual pixels

350 is approximately 1 DU. All of the analysis in our study is done at the highest resolution that is available for all fields, which is the NAME model output (0.2°latitude and 0.4°longitude). Due to the higher spatial resolution of the satellite product, we have to average the TROPOMI output of multiple pixels within each NAME grid box (on average 9 TROPOMI pixels per NAME
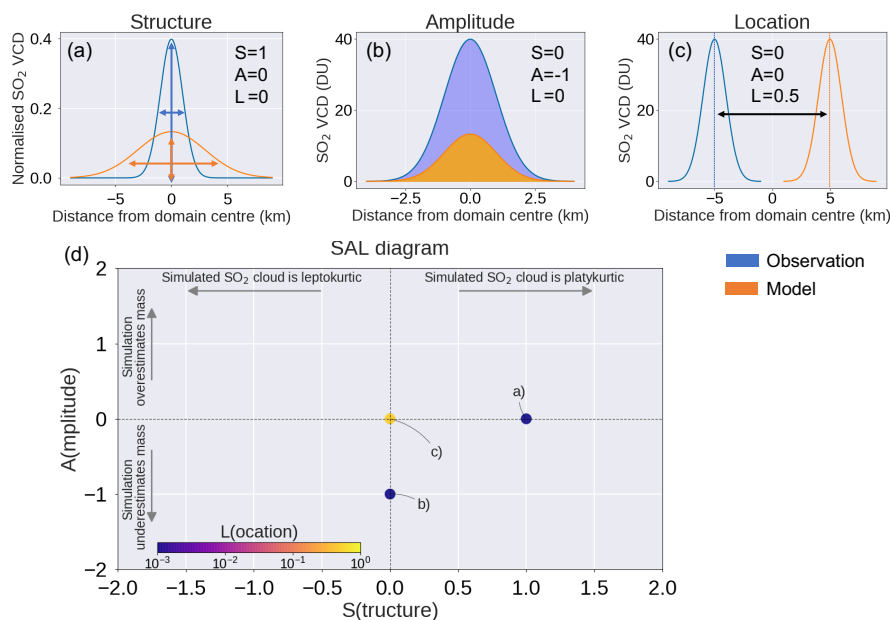
Figure 5. Schematic overview of the SAL score and its interpretation, using two cross-sections of idealised gaussian-shaped SO_2 clouds. Each panel shows the impact of an individual component of the SAL-score: a) Structure, b) Amplitude and c) Location (only the L_1 part). A negative S score indicates that the simulated SO_2 clouds are too narrow or have too high peak VCD values when compared to the observed cloud (leptokurtic). When the simulated SO_2 clouds are too wide spread or have too low peak VCD values, this is indicated by a positive S score (platykurtic). Panel d) shows an example of the SAL-score diagram with the scores of the three cases in a), b) and c) included. The horizontal axis represent the S score, the vertical axis the A score and the colour of each point represents the L score. When the simulation and observations compare perfectly, the score of each of the components is 0. The simulation and observations compare best when all the points are near the origin and have the dark purple colour.

output grid box at each given time step) to get both datasets on the same output grid. As a result, we have used a lower detection threshold of 0.3 DU when identifying all grid points that are part of a SO_2 cloud for the (re-gridded) TROPOMI retrievals and the NAME simulations. To remove additional spurious data from the TROPOMI satellite product, we also include a minimum size of each identified SO_2 cloud to be 100 km^2 (approximately the NAME grid box size at 50°N) before considering in our analysis. Simulated and observed SO_2 VCD values below either of these thresholds are excluded from all S, A, and L calculations.

To interpret the SAL-score, let us first assume a single idealised 2D-gaussian shaped cloud for both the simulated and observed SO_2 VCDs. Looking at the schematic cross-section presented in fig. 5, three characteristics are represented by the S, A and L scores. The S score compares the shapes of each individual SO_2 clouds in terms of the horizontal extent (width) and maximum concentrations within the cloud, by comparing the normalised shape of the clouds (i.e. total mass of the simulated and the observed clouds are made equal, see fig. 5a). A negative S score indicates that the simulated SO_2 clouds are too narrow

or have too high peak VCD values when compared to the observed cloud (leptokurtic). When the simulated SO_2 clouds are

365   too wide spread or have too low peak VCD values, this is indicated by a positive S score (platykurtic).

The A score represents the comparison between the simulated and the observed total mass of SO_2 within the entire studied domain and is independent on the number of individual SO_2 clouds. Negative A scores represents an underestimate of the total SO_2 mass in the simulation when compared to the observations (fig. 5b), while a positive value shows that the simulation is overestimating the total SO_2 mass in the domain.

370   Finally the L-score represents the distribution of the individual simulated and observed SO_2 clouds within the domain and consists of two parts L_1 and L_2 (Wernli et al., 2008). L_1 represents the normalised distance between the domain-averaged centre of mass of all the simulated and observed SO_2 clouds, where a higher positive value represents a larger distance between the simulated and observed domain-averaged centres of mass (see fig. 5c). In the case of multiple SO_2 clouds, L_2 represents the differences in the distribution of individual clouds around the domain-averaged total centre of mass. L_2 is calculated by

375   considering the distance between the centre of mass of each individual cloud and the total domain-averaged centre of mass. In the case of a single object, L_2 is equal to 0, as the centre of mass in the domain is the same as the centre of mass of the individual object.

When the simulation and observations compare perfectly, the score of each of the components is 0. For the S and A score the values are all between ± 2, where a value of -1 represents a factor of 3 underestimate of the simulation compared to the

380   observations and +1 represent a factor of 3 overestimate of the simulation. For the L_1 and L_2 scores, values are between [0,1], with the worst possible score being 1 representing a distance equal to the maximum distance within the domain. Similar to Wernli et al. (2008), we will present the 3 components of this metric in a SAL-diagram (fig. 5d), where the horizontal axis represent the S score, the vertical axis the A score and the colour of each point represents the L score (sum of L_1 and L_2). The simulation and observations compare best when all the points are near the origin and have the dark purple colour.

385   **3   Results**

First we qualitatively discuss the spatial pattern of the SO_2 cloud and its dispersion across the northern hemisphere during the first week after the eruption. We then discuss the FSS and the SAL-scores for the SO_2 cloud, followed by a discussion of the SO_2 mass burden evolution during the first 25 days after the eruption. A video of the volcanic SO_2 and SO_4 VCDs as simulated by NAME for the VolRes1.5 and StratProfile emission profiles can be found in the video supplements (de Leeuw,

390   2020).

3.1   Spatial pattern of the sulfur dioxide cloud

Qualitatively, the general structure of the SO_2 cloud simulated by the NAME VolRes1.5 and the StratProfile simulations compare well with the retrieved TROPOMI SO_2 VCDs during the first week after the eruption. On 23 June 2019 the TROPOMI retrievals show the split between the northern and southern branch of the SO_2 cloud, as seen in fig. 3. This observed SO_2 cloud

395   structure was strongly influenced by a low-pressure cyclone approximately 1500 km to the east of the volcano. As a result of
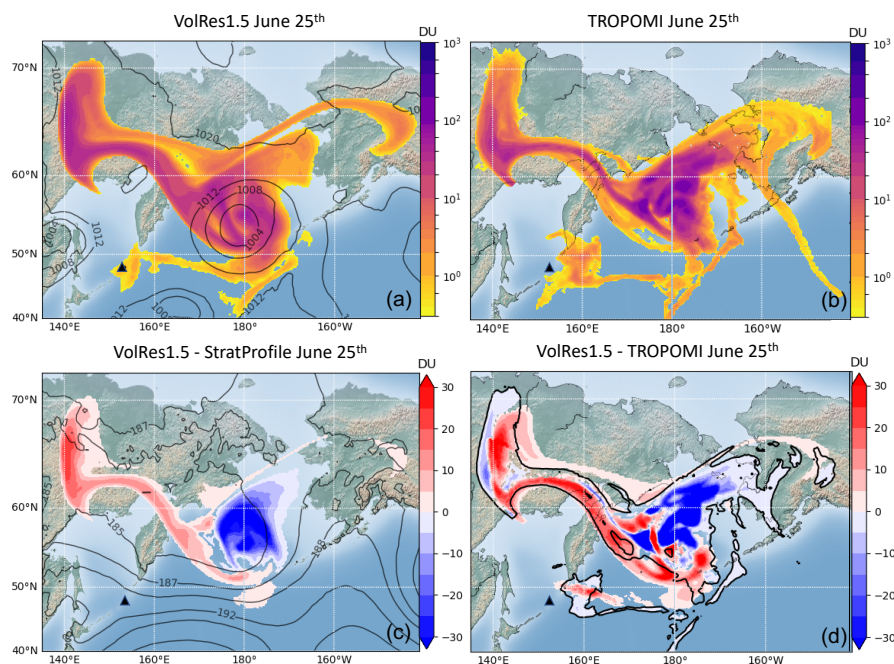
Figure 6. The spatial pattern of the volcanic cloud on 25 June 2019. The colours in panel a and b represent the vertical column density VCD for the VolRes1.5 simulation and TROPOMI retrievals respectively. The black contours in panel a) show the surface pressure, highlighting the low-pressure system in the troposphere near the centre of the cloud, east of the eruption site. Panel c) shows the difference between the VolRes1.5 and the StratProfile simulations and the black contours show the pressure at 12 km asl. The negative (blue) values indicate the part of the cloud within the stratosphere, while the positive (red) values highlight the layers within the upper troposphere. Panel d) shows the difference between panels a and b, where the contour shows the 1 DU contour for the SO_2 cloud retrieved by TROPOMI in panel b.

the low-pressure system, the volcanic cloud within the troposphere (below 11 km) moved predominantly in a south-eastward direction along the south-flank of the cyclone until it started to wrap around the centre on 23 June. For the cloud layers at higher altitudes within the stratosphere, the main wind direction was more zonal, resulting in the observed split as is visible in fig. 3. The VolRes1.5 and the StratProfile simulations show the same spatial pattern, but have different SO_2 VCDs within the
400 cloud (see e.g. fig. 3d). As expected, the StratProfile (fig. 3c) simulation shows a better agreement of the TROPOMI SO_2 VCD values within the cloud (see also section 2.3.5).

By 25 June 2019, a large part the cloud moves in a north-western direction, spreading over the Asian continent as seen in fig. 6a and fig. 6b for both the VolRes1.5 simulation and TROPOMI. Due to the variation in emission heights between the VolRes1.5 and the StratProfile simulations (fig. 2), we can identify the parts of the cloud in the NAME simulations that are mainly within
405 the troposphere and the stratosphere by comparing their differences. The results are shown in fig. 6c, which shows that the north-western part of the cloud is mainly within the troposphere, while the stratospheric parts of the cloud remain centred around the low-pressure system. Calculating the difference between the VolRes1.5 simulation and the TROPOMI retrievals in
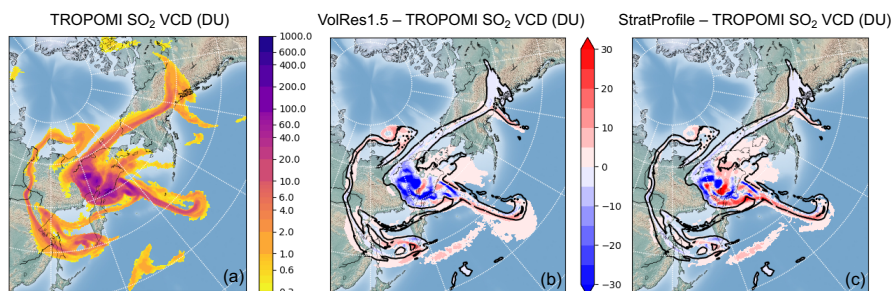
Figure 7. The spatial pattern of the volcanic SO_2 cloud as retrieved by the TROPOMI satellite for the 27 June 2019 (panel a). Panels b) and c) show the difference (in DU) with the VolRes1.5 and the StratProfile simulation respectively. Only values above 1 DU are shown. The contour shows the outline of the SO_2 cloud in TROPOMI for a VCD of 1 DU.

fig. 6d, we find that the pattern is very similar to fig. 6c. This shows that the VolRes1.5 simulation mainly overestimates the SO_2 mass of the cloud in the troposphere and underestimates the stratospheric part of the cloud.

410   On 27 June 2019, the SO_2 cloud starts to spread also at higher altitudes, leading to a complex spatial pattern as shown in fig. 7. While the large-scale structure of the cloud on 27 June has become much more complex, both the VolRes1.5 and the StratProfile simulations capture the general VCD structure of the retrieved TROPOMI cloud well. Note that the small-scale eddies observed by TROPOMI in the centre of the cloud are not simulated by NAME as a result of the limited (spatial and temporal) resolution of the NWP input. Therefore, the small-scale variability cannot be captured by the model, but instead are

415   parameterised by the diffusion parameters as a random perturbation on the wind field (see section 2.3.1). This results in the spreading of the SO_2 cloud with a smoother pattern in the NAME simulations without the high peak values. This also explains the patchy variations shown in figs. 6b and 6c within the centre of the cloud. Averaging the VCDs over the whole domain shown in fig. 7 (thereby removing the small-scale features from TROPOMI), the average VCD values for the VolRes1.5 simulation are 20% lower than measured by TROPOMI. This is also evident from the dominant blue colours in fig. 7b. For the StratProfile

420   simulation (fig. 7c) the domain-average mass is within 0.01 Tg of SO_2 of the TROPOMI SO_2 mass estimate (i.e. StratProfile SO_2 mass estimate is <1% lower than TROPOMI).

Finally, we also find a larger spread of the cloud in both the VolRes1.5 and StratProfile simulations as seen in figs. 7b and 7c by the red values outside the 1 DU TROPOMI contour. We only included the values > 1 DU in this plot for clarity of the figure. When including lower values (0.3-1 DU), the overestimation of the spread of the cloud in NAME is even larger (not

425   shown here).

3.2   Fractional Skill Score (FSS)

The VolRes1.5 and the StratProfile simulations are generally able to capture the large-scale structure of the SO_2 cloud, but differences between the simulations and the satellite retrievals occur after 4-5 days of simulation (see for example fig. 6). To determine the timescales for which the simulations show skill compared to the TROPOMI retrievals, we calculate the FSS
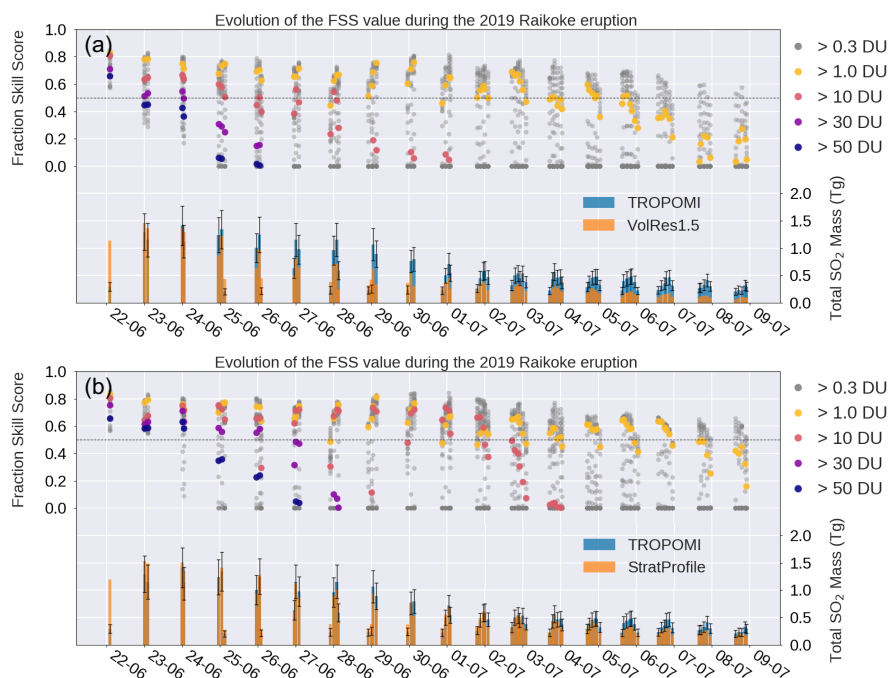
Figure 8. Time evolution of the FSS (N=1) and the SO_2 mass for each individual overpass of the TROPOMI satellite over the Raikoke cloud for a) the VolRes1.5 simulation and b) StratProfile simulation. Each annotated date represents 00UTC. Grey dots represent all concentrations between 0.3 and 100 DU, with the highest skill score for the lowest concentrations. The dashed line shows a value of FSS=0.5, which is the cut-off value for determining the skill of the simulations.

430   score for each individual overpass for a range of SO_2 VCD contours (ranging between 0.3 and 100 DU). The results for the smallest neighbourhood size N=1 (i.e. the NAME output gridbox size 0.2°latitude and 0.4°longitude) are shown in fig. 8 for (a) the VolRes1.5 and (b) the StratProfile simulation.

     The VolRes1.5 simulation is able to capture the overall outline of the cloud well for this period, but is struggling to simulate the peak VCD values within the retrieved TROPOMI SO_2 cloud. Focussing on the VCD > 1 DU points in fig. 8a, the simulation

435   has skill for up to 12.5 days after the eruption start. This shows that the simulation is capturing the overall dispersion of the cloud well, as it is able to distinguish well between areas with and without any SO_2 VCDs across the northern hemisphere. For SO_2 VCDs greater than 30 DU, which correspond to small-scale features within the volcanic cloud, the simulation has no significant skill within 2.5 days after the start of the eruption. This agrees with the fact that the VolRes1.5 simulation was not able to capture the peak values on the 25 June 2019 observed by TROPOMI as shown in fig. 6.

440   The FSS values for the StratProfile simulation (fig. 8b) reveal that this simulation performs better than VolRes1.5 and has skill on a longer timescale for all of the SO_2 VCDs. For the lower VCDs (<1 DU), the StratProfile simulation remains skilful 2 days longer than the VolRes1.5 simulation (12.5 days versus 14.5 days). For the VCDs above 30 DU, the FSS skill timescale
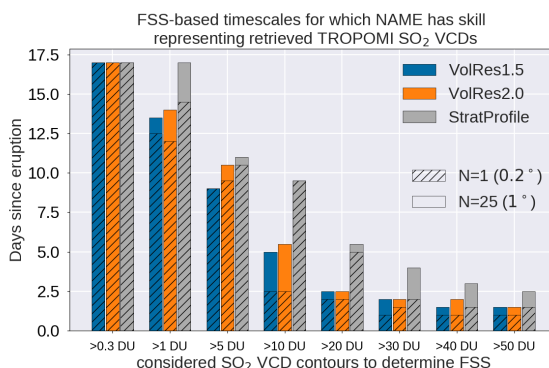
Figure 9. The timescales for which the NAME model shows skill based on the FSS, when compared with TROPOMI retrievals. The results are shown for the three simulations as discussed in section 2.3.4 and for two different neighbourhood sizes (value in brackets represent the corresponding resolution). The FSS metric is calculated only for the first 17 days of the simulation (up to 10 July), as the VCD values become too small after to give a good estimate of the FSS from the TROPOMI measurements.

has doubled compared to the VolRes1.5 simulation, showing again the importance of the emission profile on the skill of the simulation.

445   The timescales for which the NAME simulations show skill (compared to the TROPOMI retrievals) in terms of FSS are shown in table 3 and fig. 9. Independent of the neighbourhood size, the StratProfile simulation has the highest skill for all VCDs. Figure 9 shows that the StratProfile simulation is skilful on timescales twice as long for VCD values above 10 DU compared to the VolRes1.5 and VolRes2.0 simulations. Interestingly the change in neighbourhood size (i.e. averaging region) has only a limited impact on the skill timescales for low VCDs (below 5 DU). This shows that all of the simulations are able

450   to capture the horizontal extent of the SO_2 cloud well on spatial scales similar to our smallest output grid used ($0.2° \times 0.4°$) and on timescales of 2-3 weeks after the start of the eruption.

The reduction in FSS scores for high VCDs are influenced by two factors: 1) does the simulation capture high VCDs? and if so 2) is the location of the high VCD features in the SO_2 cloud (see e.g. fig. 7c) correct? Due to the dispersion of the SO_2 cloud with time, we expect a decrease in the FSS values in time for the higher VCDs as these concentrations are not present

455   anymore in either the TROPOMI retrievals nor the NAME simulations (resulting in FSS=0). For increasing VCDs, the skill timescales are therefore expected to reduce. However, compared to the VolRes1.5 and VolRes2.0 simulations, the StratProfile simulations contains higher SO_2 VCDs throughout the simulation period, resulting in relative higher FSS values.

For high VCDs, the FSS metric depends more on the used neighbourhood sizes as the corresponding SO_2 cloud features get smaller. Using a larger neighbourhood size compares the presence of small-scale features over a larger region, reducing

460   the impact of any misplacement and result in a higher FSS (see section 2.4.1). The VCD values at which model skill increases for a different neighbourhood sizes is therefore linked to a displacement error. In fig. 9, a doubling in skill timescales is found for the larger neighbourhood size (hashed versus non-hashed) at VCDs >10 DU for the VolRes1.5 and VolRes2.0 simulations, while for the StratProfile similar differences are evident for VCDs above 30 DU. This shows that the VolRes1.5 and VolRes2.0

Table 3. The FSS-based timescales estimates for which the NAME simulations have skill compared to TROPOMI at the given spatial resolution N. The given values represent the number of days after start of eruption (rounded by 0.5 days) where the FSS comparison between the NAME simulations and the TROPOMI retrievals drops below 0.5 for various neighbourhood N sizes (value in brackets shows the corresponding model resolution for which the values would be valid), maximum included vertical column density contours and NAME simulations. When calculating the daily FSS value, we only include overpasses where the satellite retrieved total mass was above 0.2 Tg to remove noise. When the model still has skill FSS > 0.6 on the last day where we could determine FSS (17 days), we represent this with a bold number, indicating that the value could be higher than what is presented here.

N=1 ($0.2° \approx 20$ km)	0.3 DU	1 DU	5 DU	10 DU	20 DU	30 DU	40 DU	50 DU
VolRes1.5	17	12.5	9	2.5	2	1	1	1
VolRes2.0	17	12	9.5	2.5	2	1.5	1	1
StratProfile	17	14.5	10.5	9.5	5	2	1.5	1.5
VolRes1.5$_{rd}$	17	12.5	9	3	2	1.5	1	1
StratProfile$_{rd}$	17	14.5	10.5	9.5	5	2	1.5	1.5
N=9 ($0.6° \approx 60$ km)	0.3 DU	1 DU	5 DU	10 DU	20 DU	30 DU	40 DU	50 DU
VolRes1.5	17	13	9	4.5	2	2	1.5	1.5
VolRes2.0	**17**	14	10	5	2.5	2	2	1.5
StratProfile	**17**	15	11	9.5	5.5	4	2.5	2
VolRes1.5$_{rd}$	17	13.5	9.5	4	2.5	2	1.5	1.5
StratProfile$_{rd}$	**17**	15	11.5	10	5.5	4	2.5	2
N=25 ($1.0° \approx 100$ km)	0.3 DU	1 DU	5 DU	10 DU	20 DU	30 DU	40 DU	50 DU
VolRes1.5	**17**	13.5	9	5	2.5	2	1.5	1.5
VolRes2.0	**17**	14	10.5	5.5	2.5	2	2	1.5
StratProfile	**17**	**17**	11	9.5	5.5	4	3	2.5
VolRes1.5$_{rd}$	**17**	13.5	9.5	5	2.5	2	1.5	1.5
StratProfile$_{rd}$	**17**	**17**	11.5	10	5.5	4.5	3	2.5
N=49 ($1.4° \approx 140$ km)	0.3 DU	1 DU	5 DU	10 DU	20 DU	30 DU	40 DU	50 DU
VolRes1.5	**17**	13.5	9	5.5	2.5	2	2	1.5
VolRes2.0	**17**	14.5	10.5	7	3	2.5	2	1.5
StratProfile	**17**	**17**	11.5	10	5.5	4.5	3	2.5
VolRes1.5$_{rd}$	**17**	14	9.5	5	2.5	2	2	1.5
StratProfile$_{rd}$	**17**	**17**	11.5	10.5	5.5	4.5	3	2.5

simulations are able to represent observed small-scale features within the SO_2 cloud for VCDs up to 10 DU at timescales less
465 than 5 days. For VCDs >20 DU these two simulations gain no additional skill with an increased neighbourhood size and show a strong reduction in skill timescales. This indicates that the high VCDs (>10 DU) observed by TROPOMI are not simulated anywhere in the SO_2 cloud at timescales longer than 5 days. For the StratProfile simulation, features with VCDs above 30
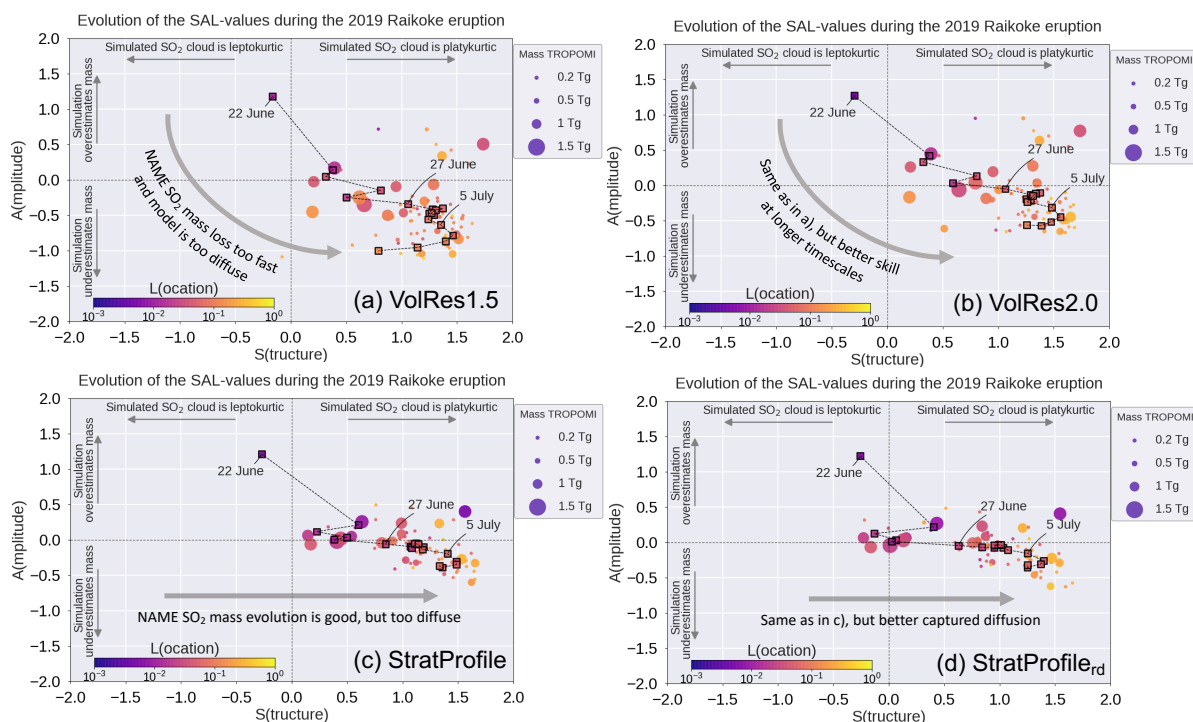
Figure 10. Time evolution of the SAL-values for 4 different NAME simulations: a) VolRes1.5, b) VolRes2.0 c) StratProfile and d) StratProfile$_{rd}$. The black dashed line shows the daily average evolution of the S and A parameters between 22 June and 10 July, while the coloured squares show the daily average values of L. The coloured dots represent the SAL-values for each individual TROPOMI overpass as shown in figure 2.

DU are still present up to 4 days. However, these features are slightly displaced, as evident from the increase in the FSS skill timescales from increasing the neighbourhood size from 0.2°to 1°.

470   On timescales longer than 5 days, all the NAME simulations show a strong diffusion in the SO$_2$ cloud (related to the diffusion parameterisations). As a result none are capturing the high VCDs retrieved by TROPOMI, which reduces the FSS quickly to 0. This shows that high VCDs within the SO$_2$ cloud, which are related to the small-scale eddies, are only skilfully simulated on timescales less than 5 days.

3.3   The SAL-score

475   Figure 10 shows the SAL-scores for all the individual TROPOMI overpasses and the daily average values for four different NAME simulations. This comparison shows the strength of the SAL-diagram to determine what aspects of the SO$_2$ cloud are captured well by the NAME simulations and where the simulations are struggling to match the TROPOMI retrievals. At the start of the eruption, all simulations are in the top half of the diagram (positive A score). This indicates that the simulations have

a larger total SO_2 mass than the TROPOMI retrievals during the first days after the eruption. This can be partly explained by
480 the presence of ash interfering with the TROPOMI retrievals (see section 3.4). Furthermore the S-values are relatively close to
0, indicating that the shape of the cloud is captured well within the simulations. The low L values throughout all the simulation
indicate that the location of the SO_2 clouds is well captured.

All four simulations shown in fig. 10 show a tendency of increasing positive S score values with time, with a strong increase
4-5 days after the start of the eruption. An increase in the S score represents an SO_2 cloud which is more widespread (platykur-
485 tic) in the simulations compared to the VCDs obtained from TROPOMI. The largest changes in the S score around 4-5 days
into the simulation are consistent with our FSS analysis where we identified that this is also the time where the VolRes1.5 and
the StratProfile simulations are also losing the skill to represent high VCDs retrieved by TROPOMI (i.e. not capturing the peak
values in the cloud).

Focussing on the VolRes1.5 and the VolRes2.0 simulations (figs. 10a and 10b), both SAL-diagrams show a similar pattern
490 (moving from the top left towards the bottom right in the diagram). Due to the total emitted SO_2 mass being greater in the
VolRes2.0 simulation, fig. 10b shows a more positive A score during the first 5 days than the VolRes1.5 simulation as the
former overestimates the total SO_2 mass retrieved by TROPOMI. After 26 June, the A score for VolRes2.0 remains close to the
A=0 line in fig. 10b, showing that the total SO_2 mass compares better with TROPOMI for the VolRes2.0 simulation than the
VolRes1.5 simulation after 5 days. For the StratProfile simulation (panel 10c), the comparison with TROPOMI is even better
495 throughout the entire simulation, as is evident by the low A score as well as the low L score. The comparison between the
StratProfile simulation and TROPOMI for each individual TROPOMI overpass (i.e. each dot in fig. 10c) is close to the A=0
line in the diagram, showing that NAME is able to capture the total SO_2 mass very well. Also a lower L score (darker colour
of the squares and circles) indicates that the model is capturing the location of the cloud even more accurately than both the
VolRes simulations. These results are consistent with the results shown in figs. 6-9.
500 Reducing the diffusion parameter by 75% (K_{meso}, see sections 2.3.1) in the StratProfile$_{rd}$ simulation (panel 10d), reveals
a relative decrease in the S score during the first week and no change in the A and L scores when compared to fig. 10c. This
behaviour is expected, as a decreased diffusion will not alter the total mass (A score) nor the centre of mass of the individual
SO_2 clouds (L score), but it will result in a more concentrated SO_2 clouds (reduction of S). As a result, the StratProfile$_{rd}$
simulation shows the best comparison with the TROPOMI retrievals for the first 5 days of the eruption. After that the S score
505 quickly increases for all the simulations independent of the diffusion parameterisation, as diffusion related to uncertainties
from the (fine-scale) meteorological conditions start to dominate the signal.

3.4 Sulfur dioxide mass burden

Figure 11a shows the SO_2 mass burden evolution calculated from the TROPOMI satellite retrievals and three NAME simu-
lations (VolRes1.5, VolRes2.0 and the StratProfile) for the 25 days between the start of the eruption and 15 July 2019. The
510 best comparison is obtained using the StratProfile simulation, which captures both the peak value and the long-term evolution
remarkably well and falls well within the uncertainty range of the TROPOMI estimate. To obtain the mass burden, we have
excluded the VCDs of TROPOMI below 0.3 DU to reduce noise but included all mass for NAME simulations as discussed in
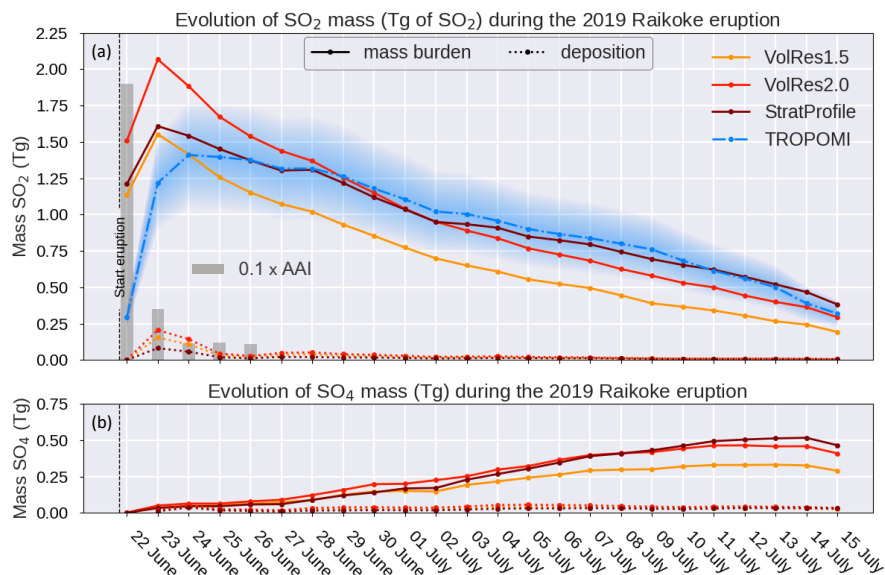
Figure 11. The daily evolution of a) the total SO_2 mass (Tg of SO_2) and b) the total SO_4 mass (Tg) for the 2019 Raikoke eruption for different ESP in NAME. We have included the TROPOMI SO_2 mass estimate (blue dashed line) as well as the evolution of 3 NAME runs: VolRes1.5, VolRes2.0 and StratProfile (see fig. 2). The dotted lines in the figures show the corresponding daily deposition of SO_2 and SO_4 (Tg) from the simulations. The peak values in the NAME SO_2 mass distribution are slightly higher than the mentioned total emission values in table 2, which is the result from applying the 15 km AK to the dispersion model data. The total SO_2 mass burden for TROPOMI is calculated using all locations where the vertical column densities are above 0.3 DU, while for the NAME simulations we include all mass. The blue shading represents the standard error estimate for the TROPOMI product. The grey bars show the TROPOMI estimated $0.1 \times$ max(AAI) value inside the volcanic cloud for the first 5 days after the eruption. The high AAI values during the first 48 hours indicate high concentrations of ash, thereby affecting the TROPOMI SO_2 retrievals during this period.

the methods (see sections 2.1 and 2.3.2). It is likely that TROPOMI underestimates the SO_2 VCDs and thus SO_2 mass during the initial phase of the eruption due to the presence of volcanic ash, which is supported by large values of AAI obtained from

515 TROPOMI during the first 2 days after the eruption (see grey bars fig. 11a and also section 2.1).

Consistent with figs. 3, 6 and 7, the VolRes1.5 simulation captures the peak in total SO_2 mass within the uncertainty of the TROPOMI estimate, but is underestimating the TROPOMI SO_2 mass between 27 June 2019 and 15 July 2019 on average by 0.3 Tg. The calculated e-folding times for SO_2 also highlight that the VolRes1.5 simulation loses SO_2 mass at a much faster rate than that calculated based on TROPOMI during the first 6 days after the eruption (e-folding time of ≈9 days versus ≈21

520 days in TROPOMI between 23-27 June 2019). As a result, this leads to a maximum underestimation of 25% (0.33 Tg) of the VolRes1.5 simulation compared to TROPOMI on 28 June. From 27 June the loss rate for both TROPOMI and VolRes1.5 are similar, with an e-folding time of ≈14-15 days, which is at the high-end of the range reported by others for eruptions of similar magnitude (e.g., Höpfner et al., 2015; Carn et al., 2016).

After 27 June 2019, the total SO_2 mass burden evolution from TROPOMI is best captured by the VolRes2.0 and the Strat-

525 Profile simulations, related to a larger amount of mass emitted into the stratosphere. From the total SO_2 mass emitted into the stratosphere calculated in table 2, we see that both the VolRes2.0 and the StratProfile respectively emit 0.2 and 0.45 Tg of SO_2 mass more into the stratosphere than the VolRes1.5 simulation. For the VolRes2.0 simulation the overall evolution of the SO_2 mass profile is similar to that obtained from the VolRes1.5 simulation (e-folding time of $\approx$9 day during the first week, e-folding time of 14-15 days afterwards). However, due to the increased total SO_2 emissions (0.5 Tg more than VolRes1.5), the SO_2

530 mass evolution of VolRes2.0 also overestimates the TROPOMI peak mass by more than 0.5 Tg on 23 June. As expected, given that TROPOMI is used as our baseline metric for initialising our StratProfile simulations, the best overall comparison with TROPOMI is obtained for the StratProfile simulation.

A possible cause for the strong reduction in total SO_2 mass during the first week for the VolRes1.5 and VolRes2.0 simulations might be too strong a conversion of SO_2 into sulfate aerosols during the start of the simulation by the processes presented in

535 section 2.3.2. To test this hypothesis, we also calculated the mass evolution of SO_4 in NAME, which are shown in fig. 11b. From this we can conclude that the chemical conversion into SO_4 is realistic within the NAME simulations. The daily rate of production of SO_4 is less than 0.03 Tg/day, which is a factor of 3 lower than the average daily decrease in SO_2 mass in the VolRes1.5 and VolRes2.0 simulations during the first week (0.1 Tg/day).

The daily total SO_2 mass deposition from the NAME simulations is shown by the dotted lines in fig. 11a. For the 23 and 24

540 June, the total daily wet deposition dominates the removal of SO_2 from the atmosphere, as it is responsible for 89-90% of the SO_2 mass reduction for the VolRes1.5, the VolRes2.0 and the StratProfile simulations. Atmospheric conditions during the first week of the eruption can explain this relatively large contribution from wet deposition. During the first week of the eruption, the SO_2 cloud is moving within a region of moist air in the warm conveyor belt on the southern edge of the cyclone (see fig. 3). This favours the chemical conversion of SO_2 into SO_4 through aqueous-phase chemistry and also the removal of SO_2 through

545 wet deposition, resulting in the peak deposition values we show in fig. 11a. The cyclone is mainly a tropospheric phenomenon and as a result wet deposition occurs mostly in the tropospheric part of the SO_2 cloud. As the VolRes2.0 simulation emits the largest amount of SO_2 into the troposphere (see fig. 2), this also explains the highest removal rate (red dotted line fig. 11a peaks at 12% of the NH-mean daily SO_2 mass burden on 23 June) and also the highest conversion rate during the first week of the simulation (evident from the largest SO_4 mass burden in fig. 11b in this period). The wet deposition is lowest for the

550 StratProfile simulation during 23 and 24 June (peaks at 4-5% of the NH-mean daily SO_2 mass burden on 23 June), as less mass is emitted into the troposphere for this profile.

The results from fig. 11 show that there is a high sensitivity of the mass burden evolution in NAME to the vertical emission profile used for this particular eruption, which straddled the tropopause. Due to different atmospheric conditions within the troposphere and stratosphere, the SO_2 mass burden evolution is different within the two layers, resulting in significant dif-

555 ferences in the total SO_2 mass burden evolution in our simulations. The average e-folding time of SO_2 is $\approx$ 10 days in the upper troposphere (e.g., Krotkov et al., 2010; Carn et al., 2016), consistent with the e-folding time simulated during the first days of the VolRes1.5 and VolRes2.0 simulations. After 10 days a large fraction of the tropospheric SO_2 mass is removed from the atmosphere through wet deposition or converted into SO_4 and the remaining signal in fig. 11 is dominated by the

stratospheric layers within the cloud. The part of the SO_2 cloud within the stratosphere is much less affected by the cyclone
560 and the environment contains much less moisture. Therefore SO_2 is removed at a much lower rate (SO_2 deposition is <1%)
and is mainly converted through the gas-phase reaction with OH, resulting in the longer e-folding time of approximately 14-15
days. The similarity in e-folding time obtained from TROPOMI and all the simulations between 27 June and 15 July suggests
that the chemistry scheme in NAME is realistic.

Overall, the total SO_2 mass burden obtained using the StratProfile emission profile compares best with TROPOMI. Based
565 on this comparison, we estimate that the 2019 eruption of Raikoke emitted approximately 0.9-1.1 Tg of SO_2 into the lower
stratosphere (11-18 km). With a maximum SO_2 mass burden of 1.5-1.6 Tg in the atmosphere, it follows that approximately
0.4-0.7 Tg was emitted into the upper troposphere (8-11 km).

4 Discussion

Our study shows that the NAME simulations compare very well with the TROPOMI satellite retrievals of the SO_2 cloud during
570 the first three weeks after the 2019 Raikoke eruption. Despite the increasing complexity of the SO_2 cloud's horizontal structure
over time, all our simulations are able to capture the outermost extent of the cloud within an accuracy of approximately 0.4°(50
km) during the first two weeks of the simulations and for up to 25 days with an accuracy of approximately 1°(100 km) (see figs.
8 and 9 and table 3). While simulated SO_2 concentrations within the cloud are strongly dependent on the ESPs, the general
dispersion patterns of the SO_2 cloud are captured very well in both the troposphere and the stratosphere for all the NAME
575 simulations performed (see figs. 3, 6 and 7). Combining this information with the comparison of the vertical profile from IASI
(fig. 4) and the included representation of the sulfur chemistry in the NAME simulations (fig. 11) gives us confidence that the
NAME model is able to reasonably accurate simulate the 3D structure of the volcanic SO_2 cloud (and consequently the SO_4
cloud) for the 2019 Raikoke eruption.

While the NAME model was not developed specifically to simulate stratospheric volcanic SO_2 clouds, our results show
580 that the model is suitable to be used by VAACs to issue forecasts on the evolution of volcanic SO_2 clouds in the upper
troposphere/lower stratosphere. Currently after a volcanic eruption, VAACs provide information on the areas in the atmosphere
where volcanic ash is forecasted up to 18 hours into the future. In the case of the Raikoke 2019 eruption, we have shown that
a similar approach to produce a forecast for the presence of a SO_2 cloud would have been accurate on this and even longer
timescales. However, future SO_2 cloud forecasts will more likely be based on designated SO_2 concentration thresholds. From
585 our simulations we found that NAME is able to capture the horizontal extent of the 1 DU VCD contour on a spatial resolution
of 0.2° × 0.4°during the first 17 days after the eruption. Assuming that the obtained VCD values are from a cloud at 12 km
altitude with a thickness of 2 km (e.g. estimated from fig. 4), 1 DU would correspond to an average SO_2 concentration of 0.02
ppm within this cloud. As reference, based on sulfur dioxide Acute Exposure Guideline Levels (AEGL) (National Research
Council Committee, 2010), an extended exposure (> 10 minutes) to SO_2 concentrations of 0.2 ppm (lowest AEGL) can lead
590 to some respiratory irritation, while concentrations above 0.75 ppm can lead to long-lasting adverse health effects. For our
example, the lowest AEGL threshold would therefore correspond to VCDs above 10 DU. We find that NAME is capable of

capturing the spatial distribution of the features within the SO_2 cloud where the VCDs are larger than 10 DU on the order of 7-10 days (see fig. 9).

Our work highlights that accurate information on ESPs are key when comparing model simulations to satellite retrievals.
595   Our analysis of the 2019 Raikoke eruption shows that the skill of the NAME simulations is strongly dependent on the emission height of the volcanic SO_2, with best results obtained when approximately two-thirds of the total SO_2 mass is emitted into the stratosphere. Interestingly while the fractional split of the mass between the stratosphere and troposphere is important, the detailed vertical distribution of SO_2 within each of these two layers has only a minor effect on model performance. To test the sensitivity of the model results to the details of the vertical distribution of the emissions within the troposphere and
600   stratosphere, we performed a simulation where we emitted 1 Tg evenly between 11-14 km and 0.5 Tg evenly between 9-11 km (not shown). The general conclusions were the same as shown for the StratProfile, illustrating that, for the 2019 Raikoke eruption, it is key to establish the fraction of the SO_2 mass that was emitted into the stratosphere.

The vertical SO_2 emission profile is also the main driver of the differences found between the NAME simulations using either the StratProfile or the VolRes1.5 vertical emission profile. For the VolRes1.5 simulations, only 43% of the total SO_2
605   mass is emitted above the tropopause as defined in the MetUM NWP, while in the StratProfile 69% of total SO_2 mass is emitted into the stratosphere. What follows is that an error in the definition of the tropopause height within the MetUM (or any other NWP) model can have a large influence on the skill of the dispersion simulations. If, for example, the MetUM model-estimated tropopause height is 2 km above the actual observed tropopause height, this would lead to a wrong placement of the majority of the SO_2 mass in the troposphere for the VolRes1.5 simulation. Using a different NWP model with a lower
610   tropopause height in the NAME simulations would result in a higher fraction of the SO_2 mass of the VolRes1.5 profile being emitted into the stratosphere and potentially give a better comparison with TROPOMI than the StratProfile estimate (which would overestimate the stratospheric SO_2 mass in that case). However, we found the average tropopause height of 11.2 ± 0.7 km diagnosed in the model at the eruption site is in good agreement with the observed tropopause height of 10.5 ± 0.7 km from a nearby radiosonde location (see fig. 2), which gives us confidence that our StratProfile emission estimates for the stratosphere
615   and troposphere are suitable and that the NAME results are not strongly biased by a wrong tropopause height within the NWP fields.

While we have investigated the impact of changing the vertical SO_2 emission profile (see fig. 2), we have not investigated the effect of any uncertainty related to the atmospheric conditions in the NWP wind fields used as input for the NAME simulation. A study by Dacre and Harvey (2018) shows that the impact of the atmospheric conditions on the NAME simulations can be
620   large, especially in conditions of large horizontal flow separation in the atmosphere. The specific atmospheric conditions for this particular eruption (i.e. the low-pressure system east of the eruption site) shows isobars that are parallel to each other during the first days after the eruption in the region of the cloud (e.g. fig. 3). Therefore, it is expected that the impact of flow separation is limited during the initial stages of the cloud evolution. After several days, the flow separation becomes more pronounced in various regions in the domain (see e.g. fig. 6). This effect is also reflected in the decrease in the S score value
625   of the SAL diagram shown in fig. 10, as trajectories start diverging in these regions of enhanced flow separation enhancing

diffusion in the model. To better understand the impact of the NWP wind field variability on our results presented here, the analysis would need to be repeated using an ensemble of NWP wind field forecasts as input for the NAME simulations.

Our study of the 2019 Raikoke eruption demonstrates the strength of the SAL-diagram for performing a comparison of model simulations with satellite observations and can help to determine potential issues. In this particular case, the NAME

630 model simulations generally tend to show increasing positive S score values for all the simulations. Partly this is related to the diffusion parameterisation in the model, which smooths the signal (i.e. random perturbation) of the small-scale eddies within the cloud that are not present in the input wind field (see sections 2.3.1). As uncertainties from the (fine-scale) meteorological conditions used as input for the simulations gradually accumulate, this leads to a larger spread in the SO_2 cloud over time than what is observed in reality. This gives the tendency for the model to be more diffuse on longer timescales, as revealed by the S

635 score increase in figs. 10a-c.

We find that the key reason for the increasing S score values on shorter timescales (i.e. 1-5 days) is related to the diffusion parameter K_{meso} used for the model simulations. NAME v8.0 uses a single value for the diffusion coefficient within the free atmosphere (see table 1). The diffusion parameter values currently used in NAME have been determined using observational datasets near the surface (Webster et al., 2018). It is therefore possible that the mesoscale diffusion values used in the model

640 might be unsuitable for the higher levels in the atmosphere, especially in the stratosphere and thereby cause too much diffusion from the start of the eruption. To test this hypothesis, we investigated several simulations with a smaller diffusion coefficient (see table 2), where we reduce the mesoscale diffusion value K_{meso} by 75%. The resulting values for the FSS-score and SAL-diagram for the StratProfile$_{rd}$ are shown in table 3 and fig. 10d and indicate that the simulations are better able to capture the structure (i.e. peak values and horizontal extent) of the cloud during the first 5 days of the simulations. It is however currently

645 impossible to determine a more precise value for the diffusion parameters, due to the lack of case studies and limited available observations for these high altitudes.

A previous study by Harvey et al. (2018) used a multi-level emulation approach to better understand the influence of model parameters on the accuracy of NAME output for volcanic ash concentration during the 2010 Eyjafjallajökull eruption. Their study showed a limited impact of the mesoscale diffusion parameter K_{meso} on their simulations for the 2010 Eyjafjallajökull

650 eruption. This limited effect of K_{meso} is partly explained by the lower resolution (40×40 km) of their model output. This leads to an averaging of small-scale eddies and a reduced impact of the diffusion parameterisation, something we also observed in our study when using a larger neighbourhood size N in our calculations of the FSS score (see fig. 10 and table 3). Furthermore, the 2010 Eyjafjallajökull emissons were at lower altitude than for the Raikoke eruption, so a larger K_{meso} might be more appropriate. However, the reduced K_{meso} values in our StratProfile$_{rd}$ simulations are within the range of realistic

655 values for the free atmosphere (see table 1 in Harvey et al. (2018)) and so this motivates more research to investigate the potential improvement of the model by having a more detailed representation of the mesoscale diffusion in the model at higher altitudes. Part of ongoing work is to investigate the impact of a new space and time-varying free-atmospheric turbulence scheme that is included in the latest version of NAME (Dacre et al., 2015), which was not available for the simulations presented in this paper.

660   The results from our work are for a single case study, as 2019 Raikoke is the first eruption of this magnitude that has been observed by the high-spatial resolution TROPOMI instrument. Nonetheless, our work shows the large potential of using TROPOMI SO_2 retrievals (in combination with the correct AKs) to identify and rectify issues in dispersion modelling efforts of volcanic eruptions. Comparing high-resolution satellite measurements and dispersion model simulations is a valuable exercise that can help improve both the volcanic dispersion modelling tools and the satellite retrievals of volcanic plumes. By combining

665   the information obtained from NAME, TROPOMI and IASI for Raikoke 2019, we are able to give a more detailed picture of the eruption source parameters and the dispersion of the volcanic SO_2 cloud than ever before. Even though we only considered this one case study, it becomes clear that improvements in ADMs simulating volcanic eruptions can be expected when more volcanic eruptions are investigated using this or similar frameworks.

       While this study has focussed almost entirely on representing the evolution of the gas-phase sulfur in the form of SO_2, it

670   is acknowledged that this is only part of the story. The Part 2 companion paper (Osborne et al., 2020) focusses on assessing the fidelity of the NAME model in representing the resulting sulfate aerosol together with volcanic ash and any confounding effects from biomass burning aerosol that were emitted into the stratosphere from an unusually strong pyrocumulus event in continental north America.

5   Conclusions

675   Volcanic eruptions can pose a large threat to society and in particular the aviation industry. In this study we simulated the 2019 Raikoke eruption using the Met Office's Numerical Atmospheric-dispersion Modelling Environment (NAME). The 21-22 June 2019 Raikoke eruption emitted 1.5 ± 0.2 Tg of SO_2 into the upper troposphere/lower stratosphere. We evaluated the skills and limitations of NAME to simulate the dispersion of the resulting volcanic SO_2 cloud by comparing our simulations to high-resolution satellite measurements from the Tropospheric Monitoring Instrument (TROPOMI). A detailed assessment of

680   the sulfate aerosol together with volcanic ash from this eruption can be found in the Part 2 companion paper (Osborne et al., 2020). Based on our analysis we conclude that:

   – NAME accurately simulates the observed location and horizontal extent of the SO_2 cloud during the first 2-3 weeks after the eruption (figs. 6 and 7). NAME performs less well when SO_2 vertical column densities (VCD) exceed 20 DU (fig. 9), which are predominantly observed as small-scale features within the SO_2 cloud during the early phases of the

685   eruption. Based on the Fractional Skill Score (FFS), we find that our simulations have skill between 12-17 days when considering the 1 DU VCD contour (table 3 and fig. 10). For VCDs larger than 20 DU, predominantly observed as small-scale features within the SO_2 cloud, the model has skill on the order of 2-4 days only.

   – Based on both the FFS score and SAL-score (fig. 10), we find that the model-simulated SO_2 cloud in NAME is more diffuse than in the TROPOMI measurements, in particular for VCDs exceeding 20 DU. The diffusion parameterisation in

690   NAME, which is developed for the lower free troposphere, results in too much horizontal spread in the lower stratosphere and therefore leads to a fast reduction of SO_2 mass concentrations in the densest parts of the eruption cloud right from

the start of the eruption. This is reflected by the high positive S score of the SAL diagram shown in fig. 10 when compared to TROPOMI. Reducing the diffusion parameters in NAME, in particular the K_{meso} parameter (see section 2.3.1), results in a better agreement during the first five days of the simulation (fig. 10d), but has no significant impact on timescales longer than that. We therefore suggest that the diffusion parameters currently used in NAME are potentially too large in the upper troposphere and lower stratosphere and different values should be considered when investigating dispersion processes near the tropopause and in the stratosphere. However, we are not able to determine exact values for the diffusion parameters on the basis of this single volcanic eruption case study with one NWP representation and one set of detailed observations. In future, as more eruption case studies become available, there is a potential to constrain the values of these diffusion parameters in order to better represent the diffusion of upper tropospheric and stratosphere volcanic SO_2 clouds in NAME and other ADMs.

– For the 2019 Raikoke eruption, we find that the skill of the model strongly depends on the eruption source parameter (ESP) used for the simulation. Using the Volcanic Response team profile (VolRes 1.5 fig. 2), we find that NAME removes too much SO_2 mass from the atmosphere during the first week of the simulations (fig. 11), resulting in a shorter e-folding time in the simulation than estimated based on TROPOMI data (e-folding time of 9 days for VolRes1.5 versus 21 days in TROPOMI between 23-27 June). A large fraction of the tropospheric SO_2 mass is removed from the atmosphere in the Warm Conveyor Belt region of the cyclone east of the eruption site during the first week of the simulation. NAME performs better with the StratProfile emission profile, where a larger fraction of the total SO_2 mass is emitted into the stratosphere (1.09 Tg versus 0.64 Tg, see fig. 2 and table 2). When emitting 0.9-1.1 Tg of SO_2 into the lower stratosphere and 0.4-0.7 Tg into the upper troposphere, we obtain the best agreement with TROPOMI, both in terms of the peak SO_2 mass burden and the e-folding time of SO_2 (e-folding time of 14-15 days).

Determining the vertical SO_2 emission profile for any volcanic eruption from observations is one of the most difficult and challenging tasks the community faces. Our analysis shows that determining the details of the vertical profiles is essential in particular for eruptions that only just straddle the stratosphere in order to accurately forecast the dispersion of volcanic SO_2. This study demonstrates that combining observational datasets with dispersion model estimates can be beneficial to obtain a more detailed estimate of the volcanic SO_2 flux. The attempts in this paper to give more details on the vertical emission profile are basic and more sophisticated near realtime estimates are currently being developed by the scientific community (e.g., Kristiansen et al., 2010; Moxnes et al., 2014; Pardini et al., 2018). With the current efforts, we expect that estimates of volcanic SO_2 fluxes will become more detailed and will very likely lead to a significant improvement of model simulations of future eruptions.

Finally, the 2019 Raikoke eruption demonstrates that volcanic eruptions of this magnitude can have a significant impact on the aviation industry. The average cruise altitudes for heavy long-haul aircraft (11.9-13.7 km) falls well within the altitudes where the volcanic SO_2 cloud for the 2019 Raikoke eruption was observed (see fig. 4). Having reliable dispersion models to simulate volcanic clouds are crucial to better understand and mitigate their potential impacts. We have shown that the FSS and the SAL-score metrics are potentially very powerful tools when assessing the skill of the model simulations in comparison

with satellite measurements. The FSS score gives insight into the timescales over which the model has skill and also shows at what resolution results are significant. The SAL-score gives a more detailed overview on three different aspects of the cloud properties (shape, location and mass) and helps to identify what aspects of the eruption cloud are well represented in a model. Using the two metrics in tandem gives a good overview on the strength and weaknesses of the simulation and helps to interpret

730   the results of the forecast model in more detail. While we have applied the metrics to the NAME model and the TROPOMI retrievals, they can also be easily applied to any combination of dispersion models and spatial observations. It could therefore also be a useful tool to inter-compare skills of satellite observation products and/or multiple dispersion models.

Code and data availability.   Code and simulation data used in this manuscript may be requested from the corresponding author and can be downloaded from https://github.com/J-de-Leeuw/Raikoke. The TROPOMI satellite data can be downloaded from the ESA website

735   (https://s5phub.copernicus.eu). I.T. and R.G. plan to archive the Oxford IASI SO_2 products; in the meantime these can made available on request from Isabelle Taylor (isabelle.taylor@physics.ox.ac.uk). Radiosonde data are available at http://weather.uwyo.edu/upperair/sounding.html. The NAME code is available under license from the Met Office.

Video supplement.   Videos of the SO_2 and SO_4 NAME VCD simulations for the VolRes1.5 and the StratProfile emission profiles can be found at http://doi.org/10.5281/zenodo.3992052. (de Leeuw, 2020)

740   *Author contributions.*   J.dL., A.S. and C.W. designed the project. J.dL. set-up and performed all the NAME simulations and analysed the results. M.O. and J.H. contributed to the scientific discussion and interpretation of the results. N.K. provided model input files for the initial NAME simulations. J.dL., N.T. and R.P. were responsible for the preparation of the TROPOMI data for the comparison with the NAME output. I.T. and R.G. processed the IASI data for the comparison. A.S., C.W., and R.G. obtained the funding for this work. J.dL., A.S. and C.W. prepared the manuscript. All the authors reviewed the manuscript.

745   *Competing interests.*   The authors do not have any conflict of interests.

Acknowledgements.   J.dL., A.S., C.W., R.G. and I.T. acknowledge funding from the Natural Environment Research Council (NERC) V-PLUS grant NE/S00436X/1. I.T. and R.G. are supported by the NERC Centre for Observation and Modelling of Earthquakes, Volcanoes, and Tectonics (COMET). N.T. acknowledges financial support from ESA S5P MPC (4000117151/16/I-LG), Belgium Prodex TRACE-S5P (PEA 4000105598) projects. Funding for PhD work for M.O. was provided by NERC through the University of Exeter, grant NE/M009416/1.

750   Contributions from J.H. and A.S. benefitted from support by the NERC ADVANCE (Aerosol-cloud-climate interactions deduced using Degassing VolcANiC Eruptions), grant NE/T006897/1. The authors would like to thank Helen Webster (Met Office) for helpful discussions on the NAME diffusion parameterisations. This work used JASMIN, the UK collaborative data analysis facility, to run all the simulations

(doi:10.1109/BigData.2013.6691556). We would like to acknowledge EUMETSAT for providing the IASI spectra; and ECMWF and CEDA for the meteorological profiles used in the IASI retrievals.

References

Ashfold, M. J., Latif, M. T., Samah, A. A., Mead, M. I., and Harris, N. R. P.: Influence of Northeast Monsoon cold surges on air quality in Southeast Asia, Atmos. Environ., 166, 498–509, https://doi.org/10.1016/j.atmosenv.2017.07.047, 2017.

Bernard, A. and Rose, W. I.: The injection of sulfuric acid aerosols in the stratosphere by the El Chichón volcano and its related hazards to the international air traffic, Nat Hazards, 3, 59–67, https://doi.org/10.1007/BF00144974, 1990.

Boichu, M., Menut, L., Khvorostyanov, D., Clarisse, L., Clerbaux, C., Turquety, S., and Coheur, P.-F.: Inverting for volcanic SO_2 flux at high temporal resolution using spaceborne plume imagery and chemistry-transport modelling: the 2010 Eyjafjallajökull eruption case-study, Atmos. Chem. Phys., 13, 8569–8584, https://doi.org/10.1175/1520-0493(1950)078<0001:VOFEIT>2.0.CO;2, https://hal.archives-ouvertes.fr/hal-00799237, 2013.

Brier, G. W.: Verification of forecasts expressed in terms of probability, Mon. Weather Rev., 78, 1–3, https://doi.org/10.1175/1520-0493(1950)078<0001:VOFEIT>2.0.CO;2., 1950.

Bundke, U., Berg, M., Gomes, R., Haywood, J., Osborne, M., Schneider, J., Schulz, C., Hermann, M., Obersteiner, F., Gehrlein, T., Bönisch, H., Zahn, A., Vernier, J.-P., and Petzold, A.: Impact of the Raikoke volcanic eruption 2019 on the Northern Hemisphere UT/LS aerosol as seen from IAGOS-CARIBIC in-situ observations, European Aerosol Conference 2020, http://eac2020.de, 2020.

Carboni, E., Grainger, R., Walker, J., Dudhia, A., and Siddans, R.: A new scheme for sulphur dioxide retrieval from IASI measurements: application to the Eyjafjallajökull eruption of April and May 2010., Atmos. Chem. Phys., 12, 11 417–11 434, https://doi.org/10.5194/acp-12-11417-2012, 2012.

Carboni, E., Grainger, R., Mather, T., Pyle, D., Dudhia, A., Thomas, G., Siddans, R., Smith, A., Koukouli, M., and Balis, D.: The vertical distribution of volcanic SO_2 plumes measured by IASI, Atmos. Chem. Phys., 16, 4343–4367, https://doi.org/10.5194/acp-16-4343-2016, 2016.

Carn, S. A., Clarisse, L., and Prata, A. J.: Multi-decadal satellite measurements of global volcanic degassing, J. of Volcanol. Geoth. Res., 311, 99 – 134, https://doi.org/https://doi.org/10.1016/j.jvolgeores.2016.01.002, 2016.

Carpenter, L. J., Fleming, Z. L., Read, K. A., Lee, J. D., Moller, S. J., Hopkins, J. R., Purvis, R. M., Lewis, A. C., Müller, K., Heinold, B., et al.: Seasonal characteristics of tropical marine boundary layer air measured at the Cape Verde Atmospheric Observatory, J. Atmos. Chem., 67, 87–140, https://doi.org/10.1007/s10874-011-9206-1, 2010.

Casadevall, T. J., Reyes, P. J. D., and Schneider, D. J.: The 1991 Pinatubo eruptions and their effects on aircraft operations, in *Fire and Mud: Eruptions and Lahars of Mount Pinatubo, Philippines*, Philippine Institute of Volcanology and Seismology Quezon City, 1996.

Corradini, S., Merucci, L., and Folch, A.: Volcanic Ash Cloud Properties: Comparison Between MODIS Satellite Retrievals and FALL3D Transport Model, IEEE Geosci. Remote S., 8, 248–252, https://doi.org/10.1109/LGRS.2010.2064156, 2011.

Dacre, H. F.: A new method for evaluating regional air quality forecasts, Atmos. Environ., 45, 993–1002, https://doi.org/10.1016/j.atmosenv.2010.10.048, 2011.

Dacre, H. F. and Harvey, N. J.: Characterizing the Atmospheric Conditions Leading to Large Error Growth in Volcanic Ash Cloud Forecasts, J. Appl. Meteor. Climatol., 57, 1011–1019, https://doi.org/10.1175/JAMC-D-17-0298.1, 2018.

Dacre, H. F., Grant, A. L. M., Harvey, N. J., Thomson, D. J., Webster, H. N., and Marenco, F.: Volcanic ash layer depth: Processes and mechanisms, Geophys. Res. Lett., 42, 637–645, https://doi.org/10.1002/2014GL062454, 2015.

Dacre, H. F., Harvey, N. J., Webley, P. W., and Morton, D.: How accurate are volcanic ash simulations of the 2010 Eyjafjallajökull eruption?, J. Geophys. Res-Atmos., 121, 3534–3547, https://doi.org//10.1002/2015JD024265, 2016.

de Graaf, M., de Haan, J. F., and Sanders, A. F. J.: TROPOMI ATBD of the Aerosol Layer Height, "http://www.tropomi.eu/data-products/level-2-products", accessed: 10-07-2020, 2016.

de Leeuw, J.: Movie of the 2019 Raikoke volcanic eruption: Sulfur dioxide and sulfate dispersion as simulated by NAME, https://doi.org/10.5281/zenodo.3992052, 2020.

Dunn, M. G.: Operation of Gas Turbine Engines in an Environment Contaminated With Volcanic Ash, J. Turbomach., 134, https://doi.org/10.1115/1.4006236, 2012.

Eckhardt, S., Prata, A. J., Seibert, P., Stebel, K., and Stohl, A.: Estimation of the vertical profile of sulfur dioxide injection into the atmosphere by a volcanic eruption using satellite column measurements and inverse transport modeling, Atmos. Chem. Phys., 8, 3881–3897, https://doi.org/10.5194/acp-8-3881-2008, 2008.

Eliaz, N., Shemesh, G., and Latanision, R. M.: Hot corrosion in gas turbine components, Eng. Fail. Anal., 9, 31–43, 2002.

Goitom, B., Oppenheimer, C., Hammond, J. O. S., Grandin, R., Barnie, T., Donovan, A., Ogubazghi, G., Yohannes, E., Kibrom, G., Kendall, J.-M., et al.: First recorded eruption of Nabro volcano, Eritrea, 2011, B. Volcanol., 77, 85, https://doi.org/10.1007/s00445-015-0966-3, 2015.

Granieri, D., Vita, F., and Inguaggiato, S.: Volcanogenic SO_2, a natural pollutant: Measurements, modeling and hazard assessment at Vulcano Island (Aeolian Archipelago, Italy), Environ. Pollut., 231, 219 – 228, https://doi.org/10.1016/j.envpol.2017.07.101, 2017.

Grégoire, B., Montero, X., Galetz, M. C., Bonnet, G., and Pedraza, F.: Mechanisms of hot corrosion of pure nickel at 700° C: Influence of testing conditions, Corros. Sci., 141, 211–220, https://doi.org/10.1016/j.corsci.2018.06.009, 2018.

Hamill, P., Toon, O. B., and Kiang, C. S.: Microphysical processes affecting stratospheric aerosol particles, J. Atmos. Sci., 34, 1104–1119, https://doi.org/10.1175/1520-0469(1977)034<1104:MPASAP>2.0.CO;2, 1977.

Harvey, N. J. and Dacre, H. F.: Spatial evaluation of volcanic ash forecasts using satellite observations, Atmos. Chem. Phys., 16, 861–872, https://doi.org/10.5194/acp-16-861-2016, 2016.

Harvey, N. J., Huntley, N., Dacre, H. F., Goldstein, M., Thomson, D., and Webster, H.: Multi-level emulation of a volcanic ash transport and dispersion model to quantify sensitivity to uncertain parameters, Nat. Hazards Earth Sys., 18, 41–63, https://doi.org/10.5194/nhess-18-41-2018, 2018.

Haywood, J. M., Jones, A., Clarisse, L., Bourassa, A., Barnes, J., Telford, P., Bellouin, N., Boucher, O., Agnew, P., Clerbaux, C., et al.: Observations of the eruption of the Sarychev volcano and simulations using the HadGEM2 climate model, J. Geophys. Res-Atmos., 115, https://doi.org/10.1029/2010JD014447, 2010.

Heard, I. P. C., Manning, A. J., Haywood, J. M., Witham, C., Redington, A., Jones, A., Clarisse, L., and Bourassa, A.: A comparison of atmospheric dispersion model predictions with observations of SO_2 and sulphate aerosol from volcanic eruptions, J. Geophys. Res-Atmos., 117, https://doi.org/10.1029/2011JD016791, 2012.

Hofmann, D. J. and Rosen, J. M.: Stratospheric sulfuric acid fraction and mass estimate for the 1982 volcanic eruption of El Chichon, Geophys. Res. Lett., 10, 313–316, https://doi.org/10.1029/GL010i004p00313, 1983.

Höpfner, M., Boone, C. D., Funke, B., Glatthor, N., Grabowski, U., Günther, A., Kellmann, S., Kiefer, M., Linden, A., Lossow, S., et al.: Sulfur dioxide (SO_2) from MIPAS in the upper troposphere and lower stratosphere 2002–2012, Atmos. Chem. Phys., 15, 7017–7037, https://doi.org/10.5194/acp-15-7017-2015, 2015.

ICAO: Handbook on the international airways volcano watch (IAVW), "https://www.icao.int/airnavigation/METP/MOGVA%20Reference%20Documents/Handbook%20on%20the%20IAVW%20Doc.9766.2019.05.08.pdf", accessed: 15-12-2019, 2019a.

ICAO: Roadmap for International Airways Volcano Watch (IAVW) in Support of International Air Navigation, "https://www.icao.int/
830   airnavigation/METP/MOGVA%20Reference%20Documents/IAVW%20Roadmap.pdf", accessed: 15-12-2019, 2019b.

Jones, A., Thomson, D., Hort, M., and Devenish, B.: The U.K. Met Office's Next-Generation Atmospheric Dispersion Model, NAME III in
Air Pollution Modeling and Its Application XVII, Springer, Boston, MA, https://doi.org/10.1007/978-0-387-68854-1_62, 2007.

Katata, G., Chino, M., Kobayashi, T., Terada, H., Ota, M., Nagai, H., Kajino, M., Draxler, R., Hort, M., Malo, A., et al.: Detailed source
term estimation of the atmospheric release for the Fukushima Daiichi Nuclear Power Station accident by coupling simulations of at-
835   mospheric dispersion model with improved deposition scheme and oceanic dispersion model, Atmos. Chem. Phys., 14, 14 725–14 832,
https://doi.org/10.5194/acp-15-1029-2015, 2014.

Kooreman, M. L., Stammes, P., Trees, V., Sneep, M., Tilstra, L. G., de Graaf, M., Stein Zweers, D. C., Wang, P., Tuinder, O. N. E.,
and Veefkind, J. P.: Effects of clouds on the UV Absorbing Aerosol Index from TROPOMI, Atmos. Meas.Tech., 2020, 1–31,
https://doi.org/10.5194/amt-2020-112, https://www.atmos-meas-tech-discuss.net/amt-2020-112/, 2020.

840   Kristiansen, N. I., Stohl, A., Prata, A. J., Richter, A., Eckhardt, S., Seibert, P., Hoffmann, A., Ritter, C., Bitar, L., Duck, T. J.,
et al.: Remote sensing and inverse transport modeling of the Kasatochi eruption sulfur dioxide cloud, J. Geophys. Res-Atmos., 115,
https://doi.org/10.1029/2009JD013286, 2010.

Kristiansen, N. I., Prata, A. J., Stohl, A., and Carn, S. A.: Stratospheric volcanic ash emissions from the 13 February 2014 Kelut eruption,
Geophys. Res. Lett., 42, 588–596, https://doi.org/10.1002/2014GL062307, 2015.

845   Krotkov, N. A., Schoeberl, M. R., Morris, G. A., Carn, S., and Yang, K.: Dispersion and lifetime of the SO_2 cloud from the August 2008
Kasatochi eruption, J. Geophys. Res-Atmos., 115, https://doi.org/10.1029/2010JD013984, 2010.

Leadbetter, S. J., Hort, M. C., Jones, A. R., Webster, H. N., and Draxler, R. R.: Sensitivity of the modelled deposition of Caesium-137 from
the Fukushima Dai-ichi nuclear power plant to the wet deposition parameterisation in NAME, J. Environ. Radioactiv., 139, 200–211,
https://doi.org/10.1016/j.jenvrad.2014.03.018, 2015.

850   Mateshvili, N., Fussen, D., Mateshvili, I., F, V., Bingen, C., Paatashvili, T., Kyröllä, E., Robert, C., and Dekemper, E.: Raikoke aerosol
clouds observed from Tbilisi, Georgia and Halle, Belgium using ground-based twilight sky brightness spectral measurements., EGU
General Assembly 2020, https://doi.org/10.5194/egusphere-egu2020-7548, 2020.

Meyer, M., Burgin, L., Hort, M. C., Hodson, D. P., and Gilligan, C. A.: Large-scale atmospheric dispersal simulations identify likely airborne
incursion routes of wheat stem rust into Ethiopia, Phytopathology, 107, 1175–1186, https://doi.org/10.1094/PHYTO-01-17-0035-FI, 2017.

855   Mittermaier, M., Roberts, N., and Thompson, S. A.: A long-term assessment of precipitation forecast skill using the Fractions Skill Score,
Meteorol. Appl., 20, 176–186, https://doi.org/10.1002/met.296, 2013.

Moxnes, E. D., Kristiansen, N. I., Stohl, A., Clarisse, L., Durant, A., Weber, K., and Vogel, A.: Separation of ash and sulfur dioxide during
the 2011 Grímsvötn eruption, J. Geophys. Res-Atmos., 119, 7477–7501, https://doi.org/10.1002/2013JD021129, 2014.

Mulena, G. C., Allende, D. G., Puliafito, S. E., Lakkis, S. G., Cremades, P. G., and Ulke, A. G.: Examining the influence of meteorological
860   simulations forced by different initial and boundary conditions in volcanic ash dispersion modelling, Atmos. Res., 176-177, 29 – 42,
https://doi.org/https://doi.org/10.1016/j.atmosres.2016.02.009, 2016.

Muser, L. O., Hoshyaripour, G. A., Bruckert, J., Horvath, A., Malinina, E., Peglow, S., Prata, F. J., Rozanov, A., von Savigny, C., Vo-
gel, H., and Vogel, B.: Particle Aging and Aerosol–Radiation Interaction Affect Volcanic Plume Dispersion: Evidence from Raikoke
Eruption 2019, Atmos. Chem. Phys., 2020, 1–27, https://doi.org/10.5194/acp-2020-370, https://www.atmos-chem-phys-discuss.net/
865   acp-2020-370/, 2020.

National Research Council Committee, U. S.: Acute Exposure Guideline Levels for Selected Airborne Chemicals: 9, Sulfur Dioxide Acute Exposure Guideline Levels., "https://www.ncbi.nlm.nih.gov/books/NBK219999/", accessed: 14-07-2020, 2010.

Oppenheimer, C., Scaillet, B., and Martin, R. S.: Sulfur Degassing From Volcanoes: Source Conditions, Surveillance, Plume Chemistry and Earth System Impacts, Rev. Mineral. Geochem., 73, 363–421, https://doi.org/10.2138/rmg.2011.73.13, https://doi.org/10.2138/rmg.2011.73.13, 2011.

Osborne, M., Malavelle, F. F., Adam, M., Buxmann, J., Sugier, J., Marenco, F., and Haywood, J.: Saharan dust and biomass burning aerosols during ex-hurricane Ophelia: observations from the new UK lidar and sun-photometer network, Atmos. Chem. Phys., 19, 3557–3578, https://doi.org/10.5194/acp-19-3557-2019, https://www.atmos-chem-phys.net/19/3557/2019/, 2019.

Osborne, M., de Leeuw, J., Beckett, F., Witham, C., Kristiansen, N., Schmidt, A., Petzold, A., Marenco, F., Buxmann, J., Saint, C., and Haywood, J.: The 2019 Raikoke volcanic eruption part 2: Particle phase dispersion and concurrent wildfire smoke emissions, Atmos. Chem. and Phys., in preparation, 2020.

Pardini, F., Burton, M., Arzilli, F., La Spina, G., and Polacci, M.: SO_2 emissions, plume heights and magmatic processes inferred from satellite data: The 2015 Calbuco eruptions, J. of Volcanol. Geoth. Res., 361, 12–24, https://doi.org/10.1016/j.jvolgeores.2018.08.001, 2018.

Pfeffer, M. A., Bergsson, B., Barsotti, S., Stefánsdóttir, G., Galle, B., Arellano, S., Conde, V., Donovan, A., Ilyinskaya, E., Burton, M., Aiuppa, A., Whitty, R. C. W., Simmons, I. C., Arason, P., Jónasdóttir, E. B., Keller, N. S., Yeo, R. F., Arngrímsson, H., Jóhannsson, P., Butwin, M. K., Askew, R. A., Dumont, S., Von Löwis, S., Ingvarsson, P., La Spina, A., Thomas, H., Prata, F., Grassa, F., Giudice, G., Stefánsson, A., Marzano, F., Montopoli, M., and Mereu, L.: Ground-Based Measurements of the 2014–2015 Holuhraun Volcanic Cloud (Iceland), Geosciences, 8, https://doi.org/10.3390/geosciences8010029, 2018.

Platt, U. and Stutz, J.: Differential Optical Absorption Spectroscopy (DOAS): Principle and Applications, Springer, Berlin, 2008.

Prata, A. J. and Prata, A. T.: Eyjafjallajökull volcanic ash concentrations determined using Spin Enhanced Visible and Infrared Imager measurements, J. Geophys. Res-Atmos., 117, https://doi.org/10.1029/2011JD016800, 2012.

Prata, A. J. and Tupper, A.: Aviation hazards from volcanoes: the state of the science, Springer, 2009.

Prata, A. T., Dacre, H. F., Irvine, E. A., Mathieu, E., Shine, K. P., and Clarkson, R. J.: Calculating and communicating ensemble-based volcanic ash dosage and concentration risk for aviation, Meteorol. Appl., 26, 253–266, https://doi.org/10.1002/met.1759, 2019.

Pyle, D. M.: Mass and energy budgets of explosive volcanic eruptions, Geophys. Res. Lett., 22, 563–566, https://doi.org/10.1029/95GL00052, 1995.

Radanovics, S., Vidal, J.-P., and Sauquet, E.: Spatial verification of ensemble precipitation: an ensemble version of SAL, Weather Forecast., 33, 1001–1020, https://doi.org/10.1175/WAF-D-17-0162.1, 2018.

Redington, A. L., Derwent, R. G., Witham, C. S., and Manning, A. J.: Sensitivity of modelled sulphate and nitrate aerosol to cloud, pH and ammonia emissions, Atmos. Environ., 43, 3227–3234, https://doi.org/10.1016/j.atmosenv.2009.03.041, 2009.

Roberts, N.: Assessing the spatial and temporal variation in the skill of precipitation forecasts from an NWP model, Meteorol. Appl., 15, 163–169, https://doi.org/10.1002/met.57, 2008.

Roberts, N. M. and Lean, H. W.: Scale-selective verification of rainfall accumulations from high-resolution forecasts of convective events, Mon. Weather Rev., 136, 78–97, https://doi.org/10.1175/2007MWR2123.1, 2008.

Robock, A.: Volcanic eruptions and climate, Rev Geophys., 38, 191–219, https://doi.org/10.1029/1998RG000054, 2000.

Sahyoun, M., Freney, E., Brito, J., Duplissy, J., Gouhier, M., Colomb, A., Dupuy, R., Bourianne, T., Nowak, J. B., Yan, C., Petäjä, T., Kulmala, M., Schwarzenboeck, A., Planche, C., and Sellegri, K.: Evidence of New Particle Formation Within Etna and Strom-

boli Volcanic Plumes and Its Parameterization From Airborne In Situ Measurements, J. Geophys. Res-Atmos., 124, 5650–5668,
https://doi.org/10.1029/2018JD028882, 2019.

Schmidt, A., Ostro, B., Carslaw, K. S., Wilson, M., Thordarson, T., Mann, G. W., and Simmons, A. J.: Excess mortality in Europe following
a future Laki-style Icelandic eruption, P. Natl. Acad. Sci USA, 108, 15 710–15 715, https://doi.org/10.1073/pnas.1108569108, 2011.

Schmidt, A., Carslaw, K. S., Mann, G. W., Rap, A., Pringle, K. J., Spracklen, D. V., Wilson, M., and Forster, P. M.: Importance of tropospheric
volcanic aerosol for indirect radiative forcing of climate, Atmos. Chem. Phys., 12, 7321–7339, https://doi.org/10.5194/acp-12-7321-2012,
2012.

Schmidt, A., Witham, C. S., Theys, N., Richards, N. A. D., Thordarson, T., Szpek, K., Feng, W., Hort, M. C., Woolley, A. M., Jones, A. R.,
et al.: Assessing hazards to aviation from sulfur dioxide emitted by explosive Icelandic eruptions, J. Geophys. Res-Atmos., 119, 14–180,
https://doi.org/10.1002/2014JD022070, 2014.

Schmidt, A., Leadbetter, S., Theys, N., Carboni, E., Witham, C. S., Stevenson, J. A., Birch, C. E., Thordarson, T., Turnock, S., Bar-
sotti, S., Delaney, L., Feng, W., Grainger, R. G., Hort, M. C., Höskuldsson, Á., Ialongo, I., Ilyinskaya, E., Jóhannsson, T., Kenny,
P., Mather, T. A., Richards, N. A. D., and Shepherd, J.: Satellite detection, long-range transport, and air quality impacts of vol-
canic sulfur dioxide from the 2014–2015 flood lava eruption at Bárðarbunga (Iceland), J. Geophys. Res-Atmos., 120, 9739–9757,
https://doi.org/10.1002/2015JD023638, 2015.

Schmidt, A., Mills, M. J., Ghan, S., Gregory, J. M., Allan, R. P., Andrews, T., Bardeen, C. G., Conley, A., Forster, P. M., Gettelman, A.,
et al.: Volcanic radiative forcing from 1979 to 2015, J. Geophys. Res-Atmos., 123, 12 491–12 508, https://doi.org/10.1029/2018JD028776,
2018.

Sears, T. M., Thomas, G. E., Carboni, E., Smith, A. J., and Grainger, R. G.: SO_2 as a possible proxy for volcanic ash in aviation hazard
avoidance, J. Geophys. Res-Atmos., 118, 5698–5709, https://doi.org/10.1002/jgrd.50505, 2013.

Shindell, D. T., Schmidt, G. A., Mann, M. E., and Faluvegi, G.: Dynamic winter climate response to large tropical volcanic eruptions since
1600, J. Geophys. Res-Atmos., 109, https://doi.org/10.1029/2003JD004151, 2004.

Solomon, S., Daniel, J. S., Neely, R. R., Vernier, J.-P., Dutton, E. G., and Thomason, L. W.: The persistently variable "background" strato-
spheric aerosol layer and global climate change, Science, 333, 866–870, https://doi.org/10.1126/science.1206027, 2011.

Stenchikov, G.: Chapter 26 - The Role of Volcanic Activity in Climate and Global Change, Elsevier, Boston, Second Edition edn.,
https://doi.org/https://doi.org/10.1016/B978-0-444-63524-2.00026-9, 2016.

Theys, N., Smedt, I. D., Yu, H., Danckaert, T., Gent, J. v., Hörmann, C., Wagner, T., Hedelt, P., Bauer, H., Romahn, F., et al.: Sulfur dioxide re-
trievals from TROPOMI onboard Sentinel-5 Precursor: algorithm theoretical basis., Atmos. Meas. Tech., 10, https://doi.org/10.5194/amt-
10-119-2017, 2017.

Theys, N., Hedelt, P., De Smedt, I., Lerot, C., Yu, H., Vlietinck, J., Pedergnana, M., Arellano, S., Galle, B., Fernandez, D., et al.: Global
monitoring of volcanic SO_2 degassing with unprecedented resolution from TROPOMI onboard Sentinel-5 Precursor, Sci. Rep., 9, 1–10,
https://doi.org/10.1038/s41598-019-39279-y, 2019.

Theys, N. e. a.: S5P ATBD of the Sulfur dioxide product, http://www.tropomi.eu/data-products/level-2-products, accessed: 17-12-2019,
2018.

Trenberth, K. E. and Dai, A.: Effects of Mount Pinatubo volcanic eruption on the hydrological cycle as an analog of geoengineering, Geophys.
Res. Lett., 34, https://doi.org/10.1029/2007GL030524, 2007.

Vaughan, G., Wareing, D., and Ricketts, H.: Lidar observations of volcanic aerosol over the UK since June 2019, EGU General Assembly
2020, https://doi.org/10.5194/egusphere-egu2020-5653, 2020.

Veefkind, J., Aben, I., McMullan, K., Förster, H., De Vries, J., Otter, G., Claas, J., Eskes, H., De Haan, J., Kleipool, Q., et al.: TROPOMI on the ESA Sentinel-5 Precursor: A GMES mission for global observations of the atmospheric composition for climate, air quality and ozone layer applications, Remote Sens. Environ., 120, 70–83, https://doi.org/10.1016/j.rse.2011.09.027, 2012.

945   Webster, H., Whitehead, T., and Thomson, D.: Parameterizing Unresolved Mesoscale Motions in Atmospheric Dispersion Models, J. Appl. Meteor. Climatol., 57, 645–657, https://doi.org/10.1175/JAMC-D-17-0075.1, 2018.

Webster, H. N., Devenish, B. J., Haywood, J. M., Lock, A. P., and Thomson, D. J.: Using plume rise schemes to model highly buoyant plumes from large fires, Int. J. Environ. Pollut., 44, 226–234, https://doi.org/10.1504/IJEP.2011.038422, 2011.

Webster, H. N., Devenish, B. J., Mastin, L. G., Thomson, D. J., and Van Eaton, A. R.: Operational Modelling of Umbrella Cloud Growth in

950   a Lagrangian Volcanic Ash Transport and Dispersion Model, Atmosphere, 11, 200, https://doi.org/10.3390/atmos11020200, 2020.

Wernli, H., Paulat, M., Hagen, M., and Frei, C.: SAL—A novel quality measure for the verification of quantitative precipitation forecasts, Mon. Weather Rev., 136, 4470–4487, https://doi.org/10.1175/2008MWR2415.1, 2008.

Whitty, R. C. W., Ilyinskaya, E., Mason, E., Wieser, P. E., Liu, E. J., Schmidt, A., Roberts, T., Pfeffer, M. A., Brooks, B., Mather, T. A., Edmonds, M., Elias, T., Schneider, D. J., Oppenheimer, C., Dybwad, A., Nadeau, P. A., and Kern, C.: Spatial and Temporal Variations in SO_2

955   and PM2.5 Levels Around Kīlauea Volcano, Hawai'i During 2007–2018, Front. Earth Sci., 8, 36, https://doi.org/10.3389/feart.2020.00036, 2020.

Wilkins, K. L., Watson, I. M., Kristiansen, N. I., Webster, H. N., Thomson, D. J., Dacre, H. F., and Prata, A. J.: Using data insertion with the NAME model to simulate the 8 May 2010 Eyjafjallajökull volcanic ash cloud, J. Geophys. Res-Atmos., 121, 306–323, https://doi.org/10.1002/2015JD023895, 2016.

960   Witham, C., Webster, H., Hort, M., Jones, A., and Thomson, D.: Modelling concentrations of volcanic ash encountered by aircraft in past eruptions, Atmos. Environ., 48, 219–229, https://doi.org/10.1016/j.atmosenv.2011.06.073, 2012.

Witham, C., Hort, M., Thomson, D., Leadbetter, S., Devenish, B., Webster, H., Beckett, F., and Kristiansen, N.: The current volcanic ash modelling set- up at the London VAAC Technical Summary (v1.6), "https://www.metoffice.gov.uk/binaries/content/assets/metofficegovuk/pdf/services/transport/aviation/vaac/london_vaac_current_modelling_setup_jan20.pdf", accessed: 27-07-2020, 2020.

965   Witham, C. S., Hort, M. C., Potts, R., Servranckx, R., Husson, P., and Bonnardot, F.: Comparison of VAAC atmospheric dispersion models using the 1 November 2004 Grimsvötn eruption, Meteorol. Appl., 14, 27–38, https://doi.org/10.1002/met.3, 2007.

Yang, K., Liu, X., Bhartia, P. K., Krotkov, N. A., Carn, S. A., Hughes, E. J., Krueger, A. J., Spurr, R. J., and Trahan, S. G.: Direct retrieval of sulfur dioxide amount and altitude from spaceborne hyperspectral UV measurements: Theory and application, J. Geophys. Res-Atmos., 115, https://doi.org/10.1029/2010JD013982, 2010.

970   Zweers, S.: TROPOMI ATBD of the UV aerosol index, "http://www.tropomi.eu/data-products/level-2-products", accessed: 10-07-2020, 2016.